Technical University of Denmark

Bachelor's Thesis

Stress and Thermal Stability of X-Ray Mirror Coatings for the ATHENA Mission

Written by

Nis Gellert s144128 _____

Jakob Korman s133943 _____

7th June 2017

Abstract

The purpose of the ATHENA mission is to observe the emitted X-ray from hot gasses orbiting a black hole, hot gasses in clusters and groups of galaxies, and the hot gasses in the intergalactic medium from the end-products of stellar evolution. This is achieved by reflecting X-ray with low and high energies at small grazing angles, using an optic module consisting of the new ESA-developed Silicon Pore Optics (SPO). The baseline coating on the SPO substrates, is a 10 bi-layer Ir/B_4C. The optic module is assembled by stacking the SPO's, where covalent bonds between each SPO substrate is achieved with an annealing procedure, which require heating the substrates to a temperature of 200 °C. This project investigates the effects, the thermal treatment has on ATHENA's mirror coating.

The XRR measurements are made with an 8 keV X-ray source, and the stress is calculated using the measured curvature scanned by a Dektak stylus profiler. With the available equipment the annealing procedure showed an improvement in the amount of X-ray reflected, and it is concluded that the iridium thickness showed no significant change. The induced stress was relatively reduced, but it was not sufficient to draw any conclusions from its cause.

Preface

This bachelor project was prepared at the Technical University of Denmark's National Space Institute. It is a coauthored paper, written by Nis Christian Gellert and Jakob Nygaard Korman.

The project involves testing the thermal stability and stress of single bi-layer coated silicon substrates. X-ray reflectivity and stress measurements are conducted on coated Ir/B_4C substrates.

We assume that the reader has knowledge in X-ray optics and physics, and understands the basics of statistical data analysis.

We thank our supervisor Desiree D. M. Ferreira, Senior Scientist, for this opportunity to work with her and this field of study. We thank Sonny Massahi, PhD student, for assisting us throughout the course of the project.

Contents

List of Figures

List of Tables

1 | Introduction

The cosmos has been investigated for thousands of years, in pursuit to solve the deepest mysteries of the Universe. In the last couple of decades, the development of advanced technology has contributed in overcoming essential challenges in the design of telescopic instruments.

The European Space Agency (ESA) is constructing a large X-ray telescope, the **A**dvanced **T**elescope for **H**igh **EN**ergy **A**strophysics (ATHENA), with planned launch around year 2028. The ATHENA mission will address how and why, does ordinary matter assemble into galaxies and galactic clusters that we see today? How do black holes grow and shape the Universe [13]? To answer these questions, ATHENA will observe the emitted X-ray from hot gasses orbiting a black hole, hot gasses in clusters and groups of galaxies, and the hot gasses in the intergalactic medium from the end-products of stellar evolution.

Detecting the X-ray portion of the electromagnetic spectrum, from specific areas of the cosmos, with immense distances, has its complications. Due the immense distance, a large optic module is needed to detect sufficient incoming X-rays. X-rays reflect at low grazing angles, giving the optic module size limitations, which results in the construction of complex mirrors.

The ATHENA mission will use the new, ESA-developed optic technology, Silicon Pore Optics (SPO) mirror modules to focus X-ray photons. The SPO is made of a 300 mm silicon wafer, with a linearly graded wedged oxide layer. They are stacked with high-precision, to form a optical module of Wolter-I configuration and its approximations [11]. A single SPO substrate is designed as shown in appendix **B** fig. 12.1, where grooves are shown cut into the underside. The grooves are 0.83 mm wide, and spaced 0.17 mm apart [25].

The baseline coating on the SPO substrates, will be an Ir/B_4C single bi-layer [6]. By applying a photoresist film on the substrate surface, and UV cure the photoresist film in a stripped pattern. The pattern will be the exact position where the ribs will touch the surface when stacking, shown on appendix **B** fig. 12.2. A reflective 10 bi-layer Ir/B_4C coating is then deposited on the substrate surface. Using a chemical procedure, the UV cured photoresist film with the coating on top, can be removed to achieve the 0.17 mm ribs on the coating.

The SPO substrates are thus all ribbed, angular wedged and coated with a pattern. The grooved ribs and stripped surface pattern without coating, both consist of a silicon oxide SiO_x surface. When substrates are stacked upon each other, covalent bonds fuse the substrates together. A strong covalent bond between each SPO substrate, is achieved with an annealing procedure, by heating the substrates to a temperature of 200 °C. Since silicon is a half metal, as the temperature rises, a polymerization reaction occurs, creating strong covalent bonds between each substrate, fusing them together.

1.1 Project objectives

In this assignment, the annealing procedure done by the European Space Agency at Cosine Research B.V. is evaluated, regarding what effects the annealing procedure will have on the Silicon Pore Optics (SPO) mirror modules. In this assignment, the robustness of the ATHENA coating to high temperatures is demonstrated.

Silicon substrates, coated with a single Ir/B_4C bi-layer, have undergone thermal tests at the Technical University of Denmark's National Space Institute. X-ray reflectivity (XRR) measurements are done before and after all thermal tests, to analyze the X-ray reflection intensity. Thin film stress measurements using Dektak stylus profilers are done before and after all thermal tests, to detect any deformation in the coating.

1.2 Project framework

The project was carried out in a systematical and consistent manner, with a project management framework in order to plan, execute and terminate the project objectives. For all experiments conducted during the course of the project, experimental manuals where made to ensure that each experiment was carried out with the same procedure. All thermal tests were carried out according to Cosine Research B. V.´s annealing procedure, approved by Boris Landgraf (BL) [7]. Weekly reports were made to control the scope, project goals and work flow. A Gantt chart was made for a visual representation of the project, with an initial work-plan and critical path. A steep learning curve and unplanned events occurred during the project, which derailed the work plan. A google-calender was created to initiate communication between co-workers, and prevent double booking on equipment.

1.3 Paper layout

Chapter 2 contains information about the ATHENA mission, the goal behind the project, the specific coating design used for the SPO's, as well as the stacking process behind the mirror optics.
Chapter 3 describes the theory and physics of X-ray, the understanding behind reflection and refraction of X-ray, and how X-ray reflectance can be calculated using the Fresnel equations.
Chapter 4 goes into detail about the coating facility and to what coating technique is used.
Chapter 5 contains all of the X-ray reflectivity measurements, information about the XRR facility, how the XRR data is interpreted using the IMD interface and with a IDL programmed script.
Chapter 6 describes the annealing procedure used by ATHENA, how the thermal tests were conducted and interpretation on the thermal heating effects.
Chapter 7 shows the stress measurements, what type of equipment was used and how the induced stress is calculated due deposition and thermal treatment.
Chapter 8 contains the main results discovered in this project, and a discussion about the work done.
Chapter 9 presents a conclusion of the work, with the results discussed in the previous chapter, together with a further studies, as to what could be the next step in this field of study.

2 | ATHENA Mission

X-ray is emitted from gasses during collision and merging of disk galaxies due shock heating. Gasses orbiting black holes emit X-ray due to loss of energy and angular momentum, which is transformed into thermal energy, et al.

The ATHENA X-ray telescope focuses on measuring the spectrum of a specific stellar object, by only measuring a narrow width of space. It will use the new SPO mirror modules to focus X-ray photons. The SPO substrates are stacked with high-precision, to form a optical module of Wolter-I configuration and its approximations. The entire optic module will consist of 120.000 SPO substrates[25], where the baseline coating on the SPO substrates is an Ir/B_4C bi-layer, with an iridium layer of 100 Å, topped with an 80 Å boron carbide layer[23]. The iridium layer will reflect X-ray in the 0.1-10 keV energy range, whereas the boron carbide will reflect X-ray in the 0.1-3 keV energy range.

2.1 Coating

ATHENA uses a baseline mirror composition consisting of an silicon(Si) substrate, and a coating containing an iridium(Ir) layer and a boron carbide(B_4C) layer. Studies have demonstrated that the use of an overcoat of a light material, onto a heavier material, can improve the reflectivity at energies between 0.5 and 5 keV, without affecting the reflectivity at higher energies[14]. The reason for adding a light material, is the fact that below the critical angle, the reflectance of a light material is higher than a heavy material, due to the extinction coefficient. The small extinction coefficient of the light material, makes it possible for high energy X-ray to penetrate down to the heavy material, and be reflected from it without considerable loss. The candidates for the light material are Si, Al, C, B and compounds like SiC and B_4C. Candidates for the heavy material are W, Re, Pt, Ni and Ir [14]. Currently the most optimal coating, is the Ir/B_4C coating. Pt/B_4C has shown to be an improvement in form of coating, but the material combination of Pt/B_4C is still unknown at present time, and is being further investigated.[6]

The baseline coating for ATHENA is the simple bi-layer with an 80 Å B_4C layer on top of a 100 Å Ir layer. Figure 2.1, shows an energy scan for Ir and B_4C. It illustrates the reflectivity each material has at low and high energies, and the combination of the two. It is clear, that the coating baseline for ATHENA favors the low energy range. The reflectance curve for the Ir/B_4C bi-layer, shows a high reflectance at low energies around 1-2 keV, due to the B_4C layer. Higher energies are reflected due to the iridium's great density. ATHENA will study X-rays in the energy range 0.1-10 keV and this combination makes it possible. This specific coating is adopted for all mirror modules at all radii[6], and the same baseline coating was used for this project.

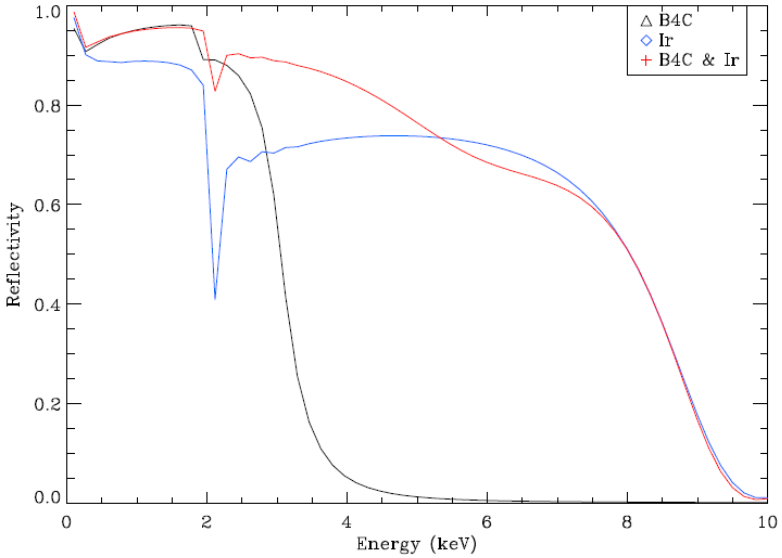

Figure 2.1: Energy scan for Ir, B_4C and the combination of the two at 8 keV

2.2 ATHENA stacking process

Strong $SiO_x - SiO_x$ covalent bonds between each SPO substrate is achieved with a direct bonding process. At room temperature, hydrogen will form as a result of adsorbed hydrophilic water molecules, on the hydrophobic SiO_x substrate surface. When two SPO substrates are stacked upon each other at room temperature, the substrates will fuse together with weak silanol bonds ($Si - O - H$). At room temperature, the following reaction takes place upon the stacking process [24]:

$$Si - O - Si + HOH \rightarrow Si - OH + HO - Si \tag{2.1}$$

Upon the annealing procedure from temperatures above 110 °C, a polymerization reaction takes place, transforming the silanol bonds into strong siloxane bonds ($Si - O - Si$). As the water molecules desorb, the strong covalent $Si - O - Si$ occur between each substrate, fusing the substrates together. The following polymerization reaction takes place at temperatures above 110 °C[27]:

$$4Si - OH + HO \rightarrow 2Si - O - Si + H_2O(g) \tag{2.2}$$

The polymerization reaction is time and temperature dependent. Surface bond energy increases with higher annealing temperatures, and as a function of cooling time to room temperature [24]. Figure 2.2 illustrates the stages of the direct bonding process.

The most stable form of adsorbed water, is as water triplets. Hydrogen-bonded water triplets are more stable than one single isolated water molecule[22], thus the absorbed water on the substrates will merge to triplets. The bond length between each $O - H$ is $\sim$ 1 Å, and the distance between each nearest neighbor $O - O$ is $\sim$3 Å[9]. Therefore, the hydrophilic substrate surfaces must be separated by up to $\sim$10 Å, for each opposing cluster of hydrogen-bonded water triplets to connect. This implies that the mean surface roughness should not be larger than $\sim$5 Å, since water triplets need $\sim$5 Å to configure, otherwise unbonded areas can occur. After the annealing process, with the polymerization reaction, the distance between each substrate will be $\sim$3 Å, since the length between a $Si - O$ is $\sim$1.6 Å.

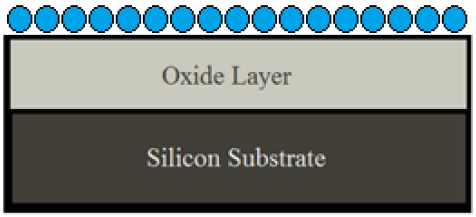

(a) Silicon substrate and oxidation layer, including absorbed water molecules

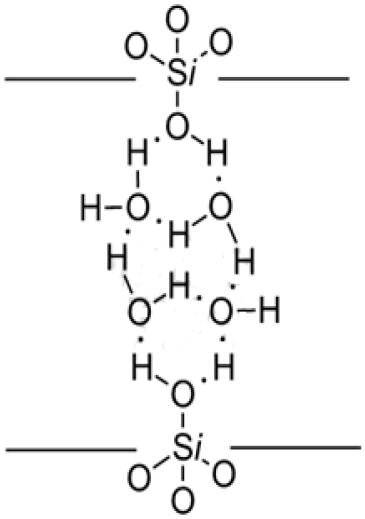

(b) The pre-bonding between two substrates at room temperature

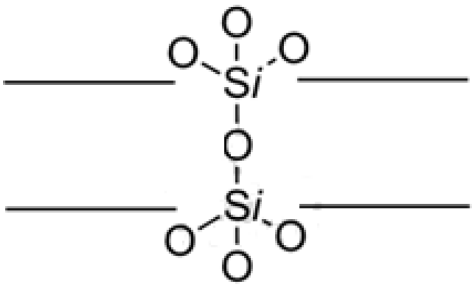

(c) The polymerization reaction bonds after the annealing process

Figure 2.2: The direct bonding process

3 | Theory

3.1 Electromagnetic waves

X-ray are high energized electromagnetic waves, in the range 100 eV to 100 keV, with short wavelengths in the range 0.01 to 10 nanometers. X-ray with photon energies lower than 5 keV are called soft X-ray, while energies above are called hard X-ray. The properties of X-ray and their penetrating ability, are used in numerous fields of study, and can be used to study the emission from celestial objects, as part of X-ray astronomy.
Electromagnetic radiation is energy that propagates through space in form of photons and waves. Electromagnetic waves consist of two waves oscillating perpendicular to each other, the electric field (E) and the magnetic field (B). This is called a transverse wave. The magnetic and electric parts of the field are in the same magnitude of strengths in order to satisfy the Maxwell equations, which specify how each one is produced from the other [12].

The $\vec{\mathbf{E}}$ and $\vec{\mathbf{B}}$ fields are in phase, while both of them reaching maxima and minima at the same points in space. Electromagnetic radiation, travels by the speed of light, and the energy which a photon has is proportional to its frequency, f, which is given by [12]:

$$E = hf = \frac{hc}{\lambda} \tag{3.1}$$

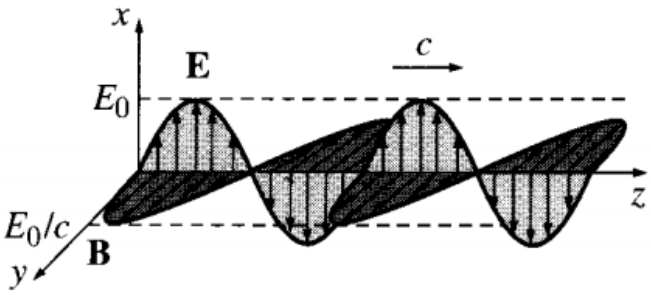

Figure 3.1: Electromagnetic Waves [12]

Upon reaching the surface of a material, the electromagnetic radiation will absorb, reflect and transmit. The intensity of the incident beam I_I, must be the sum of the intensities from the reflected I_R, transmitted I_T and absorbed I_A beams.

$$I_I = I_R + I_T + I_A \tag{3.2}$$

The optical phenomena that occurs within solid materials, are interactions between the propagated electromagnetic waves and the atoms in the material. X-ray absorbed in a material, can emit energy in the form of a characteristic fluorescent X-ray, or be scattered with and without loosing initial energy. The change in energy experienced by the electrons, depends on the radiation frequency described in equation 3.1.

For an harmonic wave moving in the direction **K**, the electric field and the magnetic field, can be described by the following complex wave function [12]:

$$\begin{aligned} \vec{\mathbf{E}}(r,t) &= \vec{E}_0 e^{i(\mathbf{k}\cdot r - \omega t)} \\ \vec{\mathbf{B}}(r,t) &= \vec{B}_0 e^{i(\mathbf{k}\cdot r - \omega t)} \end{aligned} \tag{3.3}$$

Electromagnetic waves propagate through space with the electric- and magnetic field perpendicular to each other, and to the direction of travel, but with no defined orientation. Upon reflection, the direction of polarization is defined by the plane of the surface it hits. When incident on a surface, the reflected wave will either be transverse electric (TE) polarized, transverse magnetic (TM) polarized, or partially both. The TE mode has the electric field perpendicular to the plane of incidence, and the magnetic field parallel to the plane of incidence. The TM mode has the electric field parallel to the plane of the incidence, and the magnetic field perpendicular to the plane of incidence. The reflected and transmitted amplitude expressions are different for TE or TM polarization's [10].

3.2 Snell´s law

The interaction of electromagnetic waves on a material with an oblique incidence angle $\theta_I \neq 0$, gives rise to a reflected wave,

$$\begin{aligned} \vec{\mathbf{E}}_R(r,t) &= \vec{E}_{0_R} e^{i(\mathbf{k}_R\cdot r - \omega t)} \\ \vec{\mathbf{B}}_R(r,t) &= \vec{B}_{0_R} e^{i(\mathbf{k}_R\cdot r - \omega t)} \end{aligned} \tag{3.4}$$

and a transmitted wave, shown in figure 3.2.

$$\begin{aligned} \vec{\mathbf{E}}_T(r,t) &= \vec{E}_{0_T} e^{i(\mathbf{k}_T\cdot r - \omega t)} \\ \vec{\mathbf{B}}_T(r,t) &= \vec{B}_{0_T} e^{i(\mathbf{k}_T\cdot r - \omega t)} \end{aligned} \tag{3.5}$$

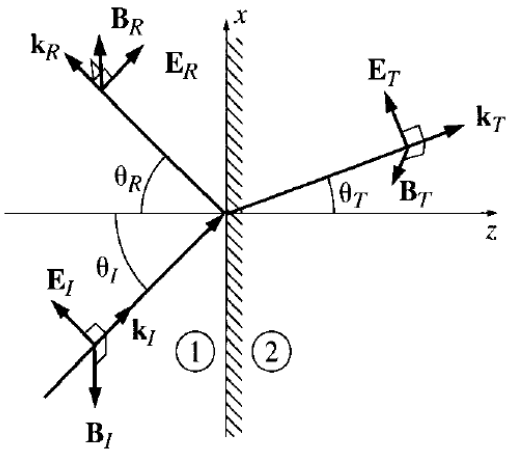

Figure 3.2: θ_I is the angle of incidence, θ_R is the angle of reflection and θ_T is the angle of transmission, also known as the angle of refraction [12]

All equations are assumed equal frequency ω, that is determined by the incident beam source. The angle of incidence is equal to the angle of reflection $\theta_I = \theta_R$, measured with respect to the normal. The transmitted angle θ_T, is given by Snell´s law [12];

$$n_1 cos\theta_I = n_2 cos\theta_T \tag{3.6}$$

The wave numbers $\mathbf{k}$, are related to Snell´s law by $k_I = k_R = \frac{n_1}{n_2} k_T$, where n is the unit-less index of refraction given by:

$$n = \frac{c}{v} \tag{3.7}$$

c is the speed of light in vacuum, and v is the beams phase velocity in the medium. Snell´s law describes the relationship between the incident angle, and the transmitted waves propagated angle in the new media, with respect to the normal. It further describes the boundary between two media with different refraction indices, though there is no overall linear relation between refractive indices and the media densities.

When an electromagnetic wave propagates into a medium with a higher electron density, and refractive index n_2, a high incident angle is needed for total external reflection, with respect to the normal. The critical angle of reflection, is the angle in which total reflection of the incident beam is achieved. Increasing the refractive index n_2, will increase the intensity of the reflected beam. When an electromagnetic waves energy is increased, the critical angle increases, with respect to the normal. X-ray are electromagnetic waves with high energy, and thus total external reflection is achieved at nearly surface parallel angles. Thus for X-ray, it is useful to define the incidence angle with respect to the media interface. This small angle is called the grazing angle. Snell´s law can be redefined to equation 3.8, where θ_I and θ_T are with respect to the interface surface:

$$n_1 cos(90 - \theta_I) = n_2 cos(90 - \theta_T) \tag{3.8}$$

3.3 X-ray Diffraction

Diffraction occurs when a wave comes across a material, that is capable of scattering the wave, and has d-spacings that are comparable in magnitude to the wavelength. X-ray diffraction gives an understanding of the size, shape and internal stress of small crystalline regions. Bragg's law describes the relation between the X-ray wavelength, and inter-atomic d-spacing to the angle of the diffracted beam. [28]

$$2dsin(\theta) = n\lambda \tag{3.9}$$

Where n is a positive integer, λ is the wavelength of the incident wave and $2dsin(\theta)$ is the extra distance the lower wave travels, which figure 3.3 illustrates.

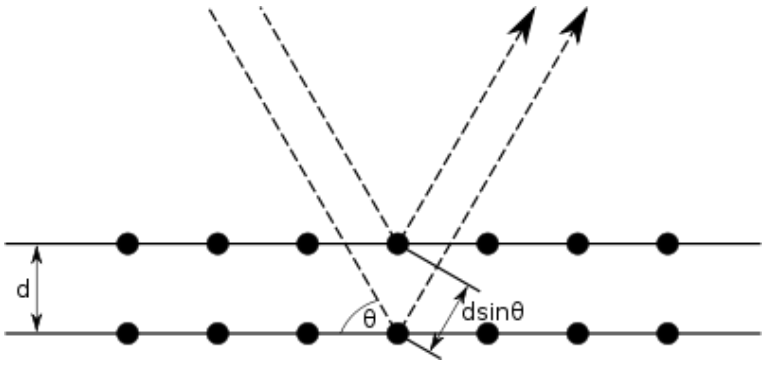

Figure 3.3: Bragg Diffraction [1]

An X-ray diffraction pattern occurs, when measuring the intensity of scattered waves as a function of the scattering angle. The strong intensities that are obtained are known as Bragg peaks. These peaks are located at the points, where the scattering angles satisfy the Bragg condition.
X-ray diffraction appears when X-ray with wavelength equal to atomic d-spacings, is scattered by the atoms in a crystalline grid and, therefor creates constructive interference.There exist two types of interference: constructive and destructive. Destructive interference takes place when two waves are not in phase with each other, thus cancelling out. Constructive interference transpires when two waves are in phase with each other, resulting in one larger wave.

Bragg's law is satisfied when the distance $2dsin(\theta)$ is equal to an integer multiple of the wavelength, which leads to constructive interference. The constructive interference results in high intensity peaks.

3.4 Interface and surface roughness

For an electromagnetic wave with an effective area, the amount of photons, $N > 1$, that are incident, will each follow the law of reflection, eq. 3.6. The surface roughness of the medium determines the orientation of the incident beams normal to the surface. A smooth surface leads to a type of reflection known as specular reflection, where all parallel incident beams are parallel when reflected. A rough surface leads to a reflection type known as diffuse reflection or non-specular reflection, shown in figure 3.4.
The surface roughness is obtained with different methods of treatment. The induced roughness on the thin film substrates used in the ATHENA mission, depend on several preparation variables [5]. Due to coating, stresses are induced in the film. Intrinsic stresses result from individual deposited grains cohesion and vacancies, where tensile and compressive stresses are generated. Interface stresses rise as the crystal lattice between deposited layers are forced to line up [17]. Extrinsic

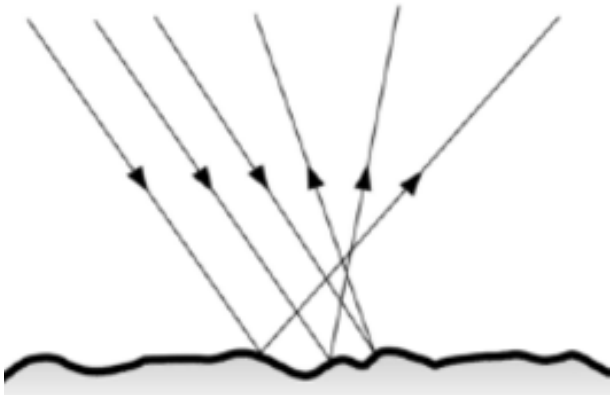

Figure 3.4: Non-specular reflection [2]

thermal stresses results from deposited layers with inhomogeneous thermal expansion coefficients, resulting in tensile and compressive stresses induced in the film [20]. The different induced stresses can alter the substrates curvature, and thus also change the surface roughness. Excessive film stress can lead to cracking. The curvature of a substrate can be calculated using Stoney´s equation 3.10, which relates to the induced stress after deposition [21].

$$\sigma = \frac{1}{6}(\frac{1}{R_{post}} - \frac{1}{R_{pre}})\frac{E}{1-v}\frac{t_s^2}{t_f} \tag{3.10}$$

Where:

- σ = Stress in the film, after deposition
- R_{pre} = Substrate radius of curvature before deposition
- R_{post} = Substrate radius of curvature after deposition
- E = Young's modulus
- v = Poisson's ratio
- t_s = Substrate thickness
- t_f = Film thickness

The substrates radius of curvature is calculated using equation 3.11, where the height of the substrate is expressed as a continuous function of distance along the substrate, $y = f(x)$ [21].

$$R(x) = \frac{(1 + y'^2)^{\frac{3}{2}}}{y''} \tag{3.11}$$

where $y' = dy/dx$, and $y'' = d^2y/dx^2$, which is calculated using a 5th order polynomial fit by the method of least squared. The difference between the pre-deposition radius and post-deposition radius, is the film induced stress, which relates to the surface roughness.

3.5 Fresnel equations

Using Snell´s law and Maxwell´s equations [12], the amount of electromagnetic waves reflected and transmitted from a surface can be calculated. Rewriting Snell´s law to eq. 3.12:

$$E_I n_1 Sin(\theta_I) = E_R n_1 Sin(\theta_R) E_I Sin(\theta_I) - E_R sin(\theta_R) = E_T n_2 Sin(\theta_T) \tag{3.12}$$

The relative reflected and transmitted intensity can be calculated, with respect to the incident intensity:

$$\begin{aligned} r &= \frac{E_R}{E_I} = \frac{Sin(\theta_I) - n_2 Sin(\theta_T)}{Sin(\theta_I) + n_2 Sin(\theta_T)} \\ t &= \frac{E_T}{E_I} = \frac{2Sin(\theta_I)}{Sin(\theta_I) + n_2 Sin(\theta_T)} \end{aligned} \tag{3.13}$$

Equation 3.13 is known as the Fresnel equations for a TE polarization. The Fresnel equations provides a unit-less integer, which describe the relative reflected- and transmitted amplitudes [23].

4 | Reflective Thin Film Deposition

For the purpose of this project, silicon substrates are coated with a single Ir/B_4C bi-layer. All samples are coated in the multi-layer coating facility, known as the Multilab, located at the Technical University of Denmark's Space Institute. The coating facility consists of a vacuum chamber, where substrates are mounted on plates that are placed on a rotating ring, which uses a direct-current magnetron-sputtering technique as coating method, shown in figure 4.1. The magnetron sputtering technique is a process where particles are ejected from solid targets, onto a substrate, due to the bombardment of ionized gasses on the target surface.

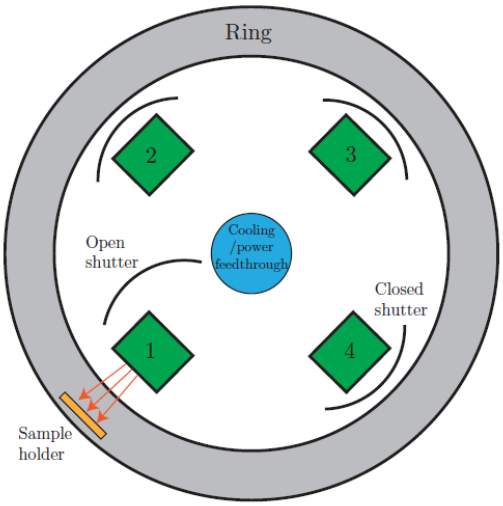

(a) Coating chamber in Multilab

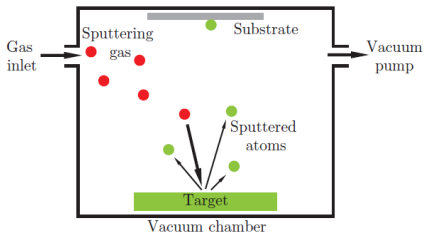

(b) Magnetron sputtering technique

Figure 4.1: Sketch of coating facility and process [23]

Instead of ATHENA´s SPO substrates, a cheaper polished silicon film is used as substrate. The target materials used were iridium and boron carbide, to create the same baseline coating composition as ATHENA. To achieve a similar deposited thickness, a calibration of the coating chamber was done. A 10 bi-layer Ir/B_4C was deposited on a silicon substrate. The sample was measured using an X-ray reflectivity technique, and compared to a model simulated in IMD to determine the deposited thickness.

The deposited thickness is determined by the velocity of the rotating ring. The coating ring is divided into 668000 angular steps, where the velocity of the rotating ring is described as the number of steps per second, defined in the coating script appendix **A** fig. 11.2. The deposition rate can thus be calculated to achieve a specific thickness.

26 silicon substrates are coated to analyze the X-ray reflection intensity, defined as witness samples. 13 silicon substrates are produced to detect any deformation in the curvature, defined as stress samples. The stress samples are slightly smaller in width. The deposition rate in the coating script, appendix **A** figure 11.1, was set to achieve an iridium thickness of 100 Å and boron carbide thickness of 80 Å. The samples were mounted on plates as shown on figure 4.2, and placed on the rotating ring in the coating chamber.

Figure 4.2: Left: Plate B15, stress samples S0902-S0914.
Right: Plate B3, witness samples Si6357-Si6382

The base pressure was $2.1 \cdot 10^{-6}$ Torr prior to deposition. High purity argon (Ar) was used as sputter gas, with a constant Ar pressure ~ 2.5 mTorr and a flow of 76.5 SCCM (Standard Cubic Centimeter pr. Minute). Vertical magnetron cathodes pointing outwards in the circular vacuum chamber, attached to a powerful DC power supply, creates an electric field in front of the target, ionizing the argon gas ejected into the chamber. The cathode attracts the positively charged argon atoms, accelerating them towards the target. The argon atoms collide with the target, ejecting matter atom-by-atom from the target, towards the silicon witness- and stress sample substrates, thus depositing angstrom thick layers.

5 | X-ray Reflectivity Measurements

During the project, 26 witness samples were coated and used for X-ray reflectivity measurements. The idea behind these experiments, is to determine the coating properties on every sample, and if it is consistent before and after heating. The XRR facility consists of an X-ray generator, 3 slits, 2 evacuated tubes, a monochromator, filters, a sample platform placed on a stage and a position sensitive linear detector, shown in figure 5.1.
The X-ray photons are generated from a rotating copper-anode. Along the z-axis, shown in figure 5.1 after the X-ray generator, are two slits, the monochromator, an attenuator (filter) and one more slit before hitting the sample platform. The first two slits direct the beam into the monochromator, which consists of two germanium crystals. The two crystals are placed in an angle where the Bragg reflection only allows photons around the copper $K_\alpha 1$ emission line, equivalent to 8.047 keV.
The beam continues to go through the attenuator and one more slit, to make sure that there isn't any unwanted reflections from the monochromator, and to ensure a narrow bandwidth.

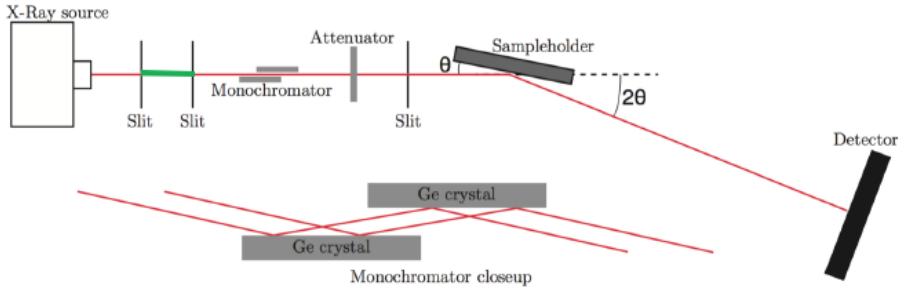

Figure 5.1: XRR-facility design [23]

Each sample is mounted on a platform, consisting of a ceramic material. The platform has a little area marked, to ensure the samples are mounted at the same spot, and it's connected to a pump which makes sure the samples stick. During the course of this project, no experiments were conducted without disposable gloves. The experimental setup is shown in appendix **I**. The platform is centered and mounted on a stage, which can rotate in an angle θ, and move in the direction of x, y and z. After the platform, further along the z-axis is the detector. The detector is a 10 cm wide 2D argon/methane-gas detector, mounted on a rotating stage of 2θ. It is possible for the detector to move 90° around the sample platform, keeping focus on the same spot. The detector has 2000 channels along the x-axis, though only 100 channels are used during the reflectivity experiment.

For each measurement, an initial alignment of the sample with respect to the incoming beam is made. The alignment is done by following the XRR manual [16] and controlled by 3 Cartesian coordinates: thx, thy and th.

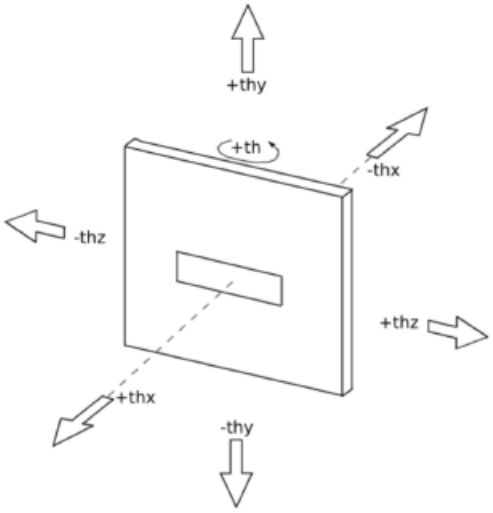

Figure 5.2: Movement of the sample platform [23]

The XRR-measurements required a script to run each measurement, shown in appendix **F**. Each scan is done from 0-4°grazing angle, and is divided into different intervals. For every interval a filter is submitted to make sure, that the detector does not reach saturation point. Since all the samples were coated together, the same XRR-measurement script was used.

5.1 Data interpretation and analysis

The data generated from the X-ray facility provides a data file which includes the relative reflected intensity, at specified incident angles. The following fig. 5.3, shows the measured reflectivity versus the grazing angle, from an XRR measurement with sample Si6372.

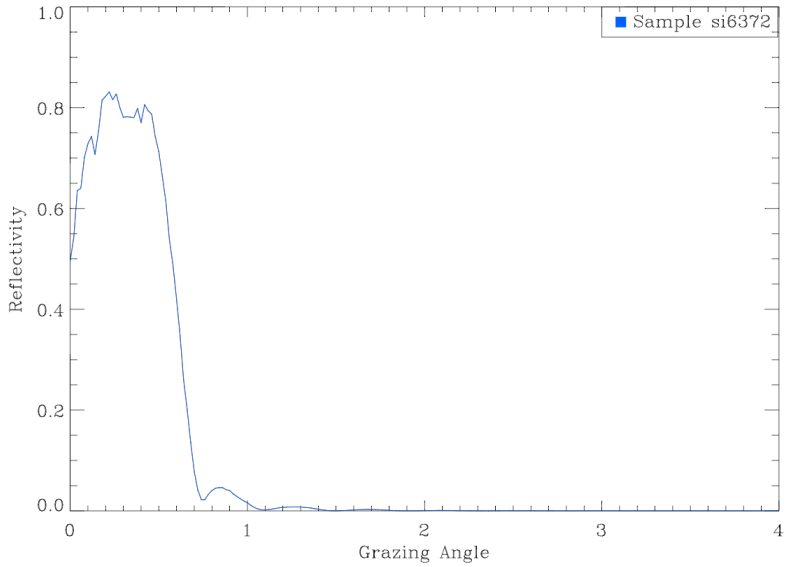

Figure 5.3: XRR output, sample Si6372

The data is shown to be very skewed to the right, which is expected since X-ray

reflects at small grazing angles. Under the critical angle $\theta \sim 0.45°$, the intensity of the reflected beam $I_R \sim 80\%$ of the incident beam I_I. Above the critical angle, the reflectivity drops drastically due to the X-ray absorption and transmission in the sample. To interpret the data in descriptive and frequentist statistic terms, the normality of the data assessed. The following fig. 5.5 shows a QQ-plot for sample Si6372, generated in RStudio.

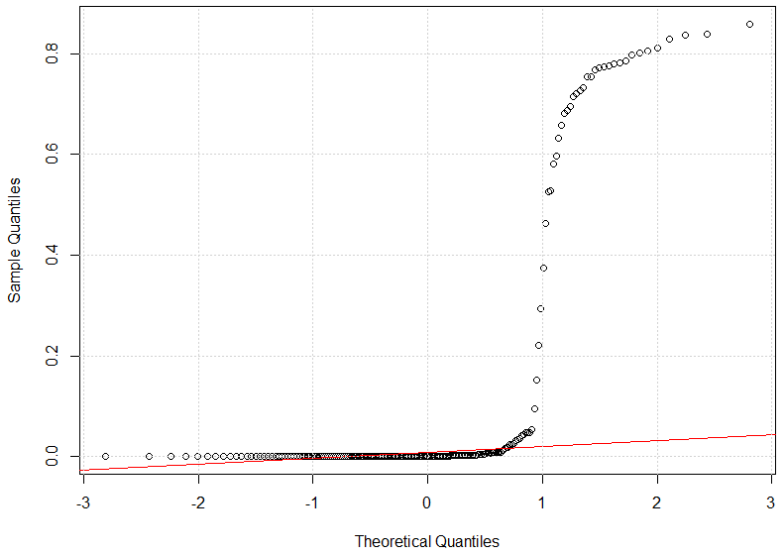

Figure 5.4: QQ-plot, sample Si6372

The QQ-plot shows that the data does not support normality, and is very right skewed, which suggests a data transformation. The log-transformation can be used to make highly skewed distributions less skewed. The following fig. 5.5 shows a QQ-plot for sample Si6372 with a logarithmic reflectivity.

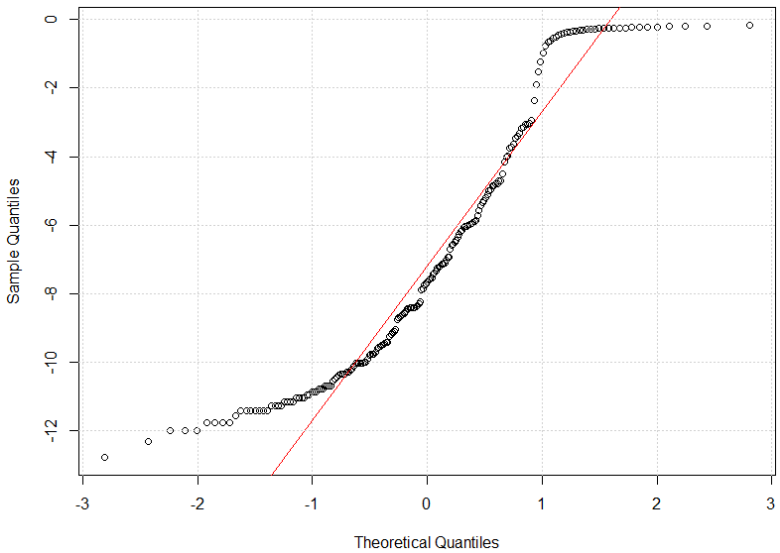

Figure 5.5: Log transformed QQ-plot, sample Si6372

The QQ-plot shows that the data is more normalized with a log transformation, but is still light-tailed, which could suggest another probability distribution. Figure 5.6 shows the output data from the XRR measurement with sample Si6372, where the reflectivity is log-scaled.

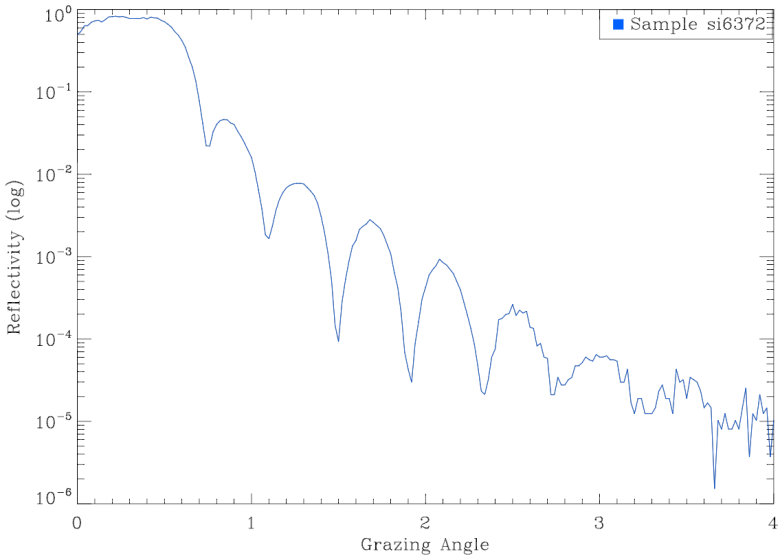

Figure 5.6: XRR with logarithmic y-axis, sample Si6372

With a log transformed reflectivity, a clearer oscillation of the intensity at different angles is shown, displaying the Bragg peaks. A log-transformation is thus sufficient.

5.2 Data analysis using IMD interface

During the course of this project, the software IMD is used to model and analyze the properties of arbitrary layered structured films. IMD is a software written in the IDL scientific programming language, which includes a user-friendly interface. The software can be used to simulate a variety of model configurations, including various parameters, variables and properties. The specular reflection is simulated using IMD´s interface, with a model configuration consisting of a single bi-layer Ir/B_4C at 8.047 keV, with the grazing incidence angle interval $\theta_I = 0 - 4$, and an instrumental angular resolution 0.007. The substrate is a silicon substrate with an initial surface roughness $\sigma_{Si} = 2.5$ Å. The iridium layer is set with a thickness $z_{Ir} = 100$ Å and a roughness $\sigma_{Ir} = 2.5$ Å. The boron carbide layer is set with a thickness $z_{B_4C} = 80$ Å, and a roughness $\sigma_{B_4C} = 2.5$ Å. The optical constants for the materials used in the simulations, have been made by the Center for X-Ray Optics and Lawrence Livermore National Laboratory.

With the calibration of the coating chamber, and the initial substrate surface roughness, these parameters are thus expected to be existent in the produced samples. Figure 5.7 shows the expected spectral reflectivity simulated using IMD´s interface, including the measured reflectivity for sample Si6372.

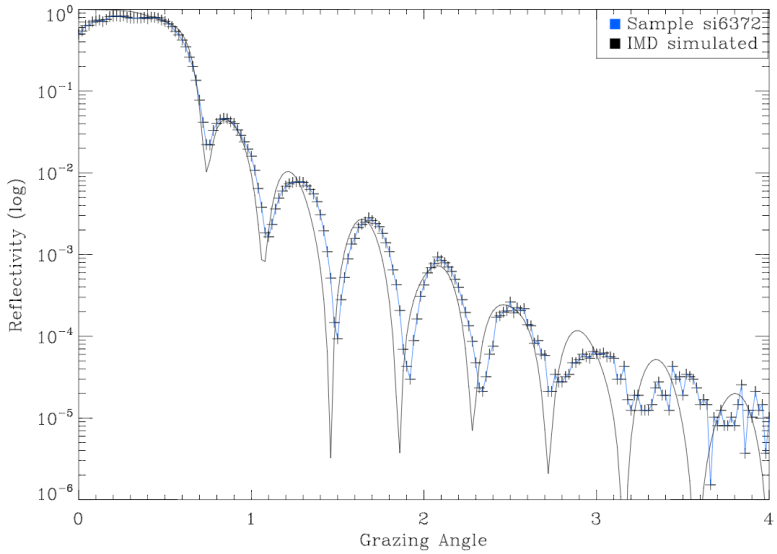

Figure 5.7: Expected vs Observed, sample Si6372

It is noticed that the expected and observed Bragg peaks are shifted and not of equal magnitude. This suggests that the coating of sample Si6372, is not the expected.

5.3 Data analysis using IMD

For this project, a script is created to simulate the best fit for the data, to determine the thickness and roughness for each layer. This is done with the IDL script shown in appendix **J**, which is run through the IMD terminal. The script is built with a combination of for-loops, to brute force calculate multiple IMD simulations with various combinations of thicknesses and roughness's. The substrates roughness is locked to its initial 2.5 Å. The interval for the Ir and B_4C thickness went from 0-200 Å, and the roughness 2-7 Å. The Fresnel function ran for each loop, and calculated the reflectively with the given parameters, for grazing 0-4°. For each Fresnel calculation, a Chi-square test is conducted to test the goodness of fit between the observed XRR data and the expected theoretical data. The Chi-square values is calculated using equation 5.1.

$$\chi^2 = \frac{(Observed - Expected)^2}{Expected} \tag{5.1}$$

The expected values for each sample is:

- B_4C thickness = 80 Å
- B_4C roughness = 2.5 Å
- Ir thickness = 100 Å
- Ir/B_4C roughness = 2.5 Å

Figure 5.8 shows the expected plot, the measured XRR data for sample Si6372 and the best IMD fit:

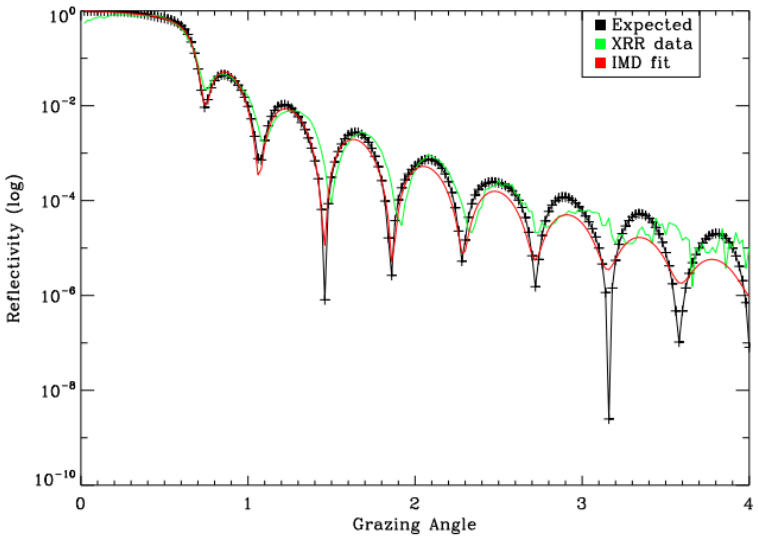

Figure 5.8: Plot showing expected with XRR data and the best fit for sample Si6372

Observing figure 5.8, it is noticed that the XRR data does not lie completely on top of the expected plot. This indicates that sample Si6372 has a change in both thickness and roughness. The calculated best fit gave the following values with a $\chi^2 = 154.35$:

- B_4C thickness = 0 Å
- B_4C roughness = 2.75 Å
- Ir thickness = 100 Å
- Ir/B_4C roughness = 4.5 Å

A B_4C thickness of 0 Å seems highly unlikely, since the coating process aimed for an 80 Å thickness. The Ir thickness of 100 Å matches the expected value, indicating that the coating process is successful. The B_4C roughness of 2.7 Å and the Ir/B_4C interface roughness of 4.5 Å is reasonable, but it is insufficient to draw any assumptions based on figure 5.8.

Figure 5.9 is a plot for each parameter vs its Chi-square value. This will give a visual interpretation of the parameters.

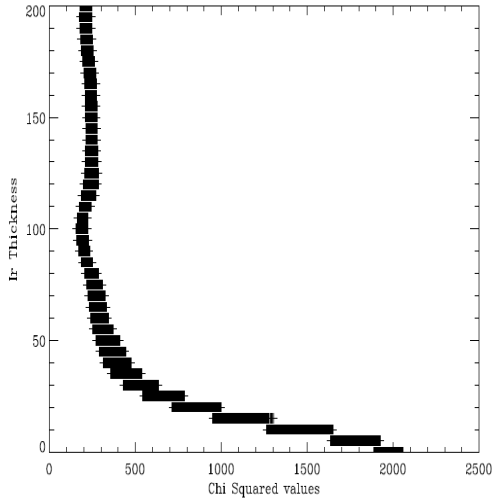

(a) Sample Si6372 Ir thickness in Å

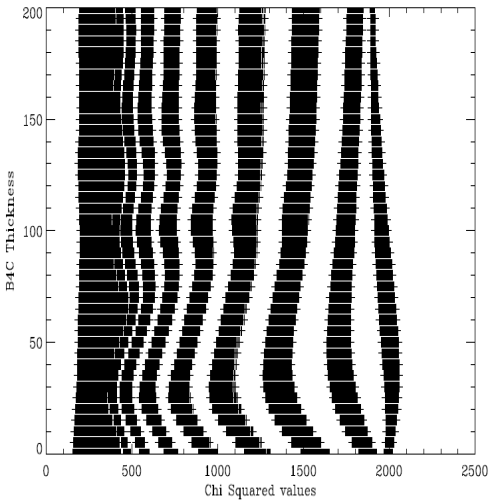

(b) Sample Si6372 B_4C thickness in Å

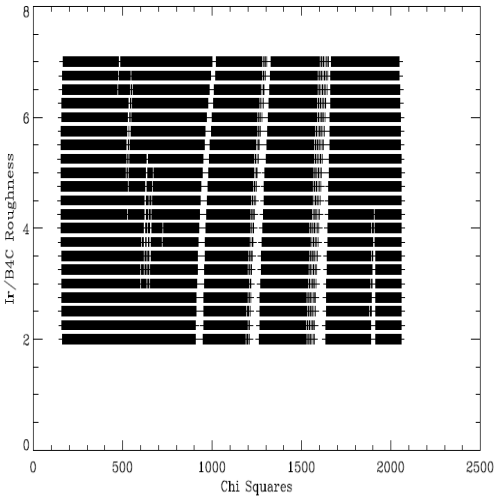

(c) Sample Si6372 Ir/B_4C roughness in Å

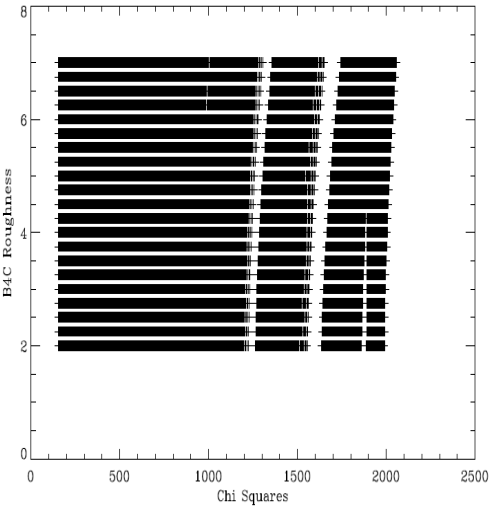

(d) Sample Si6372 B_4C roughness in Å

Figure 5.9: Chi-square plots, sample Si6372

It is noticed, that the only variable able to be constrained is the Ir thickness. The other parameters can not be constrained, which explains the calculated values for the best fit. It is not possible to determine the B_4C thickness, B_4C roughness and Ir/B_4C interface roughness, by visually studying the graphs. As explained in section 2.1, B_4C should not be detected with an 8 keV source, since it is practically transparent. This could explain why the B_4C layer is not able to be constrained. Data effected by the incident beams footprint is observable in figure 5.8, from 0-0.4°. The footprint describes the area where the beam is incident, as shown in **Appendix E**. It will result in less reflectively if the area is larger than the sample. The footprint is calculated using eq. 5.2.

$$D = \frac{d}{sin(\theta)} \tag{5.2}$$

The footprint D, is the illuminated area, to the specific angle θ and beam width d. The angle θ where the footprint is larger than the sample, is calculated to:

$$\theta = \frac{0.0012m}{0.07m} \sim 0.1^{\circ} \tag{5.3}$$

The XRR data is effected by the footprint from 0 to 0.1°. Further more, there is

an uncertainty of 0.2°on the facility, and therefore the data from 0-0.3°is removed. Removing this data results in a more precise IMD fit, shown in figure 5.10.

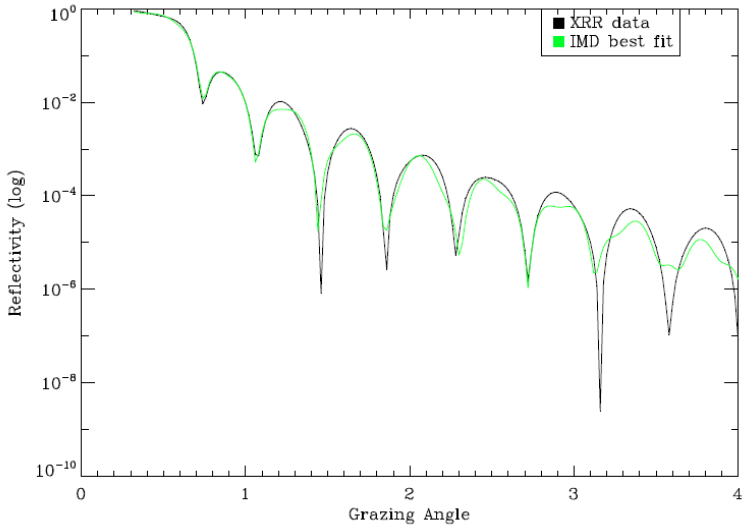

Figure 5.10: Sample Si6372 without the footprint

Figure 5.10 shows sample Si6372 without the footprint. Neglecting the footprint results in Chi-square $\chi^2 = 0.07$ for the IMD fit, which is less than the model that included the data effected by the footprint. Following figure 5.11 shows visual interpretation of the calculated Chi-square values without the footprint.

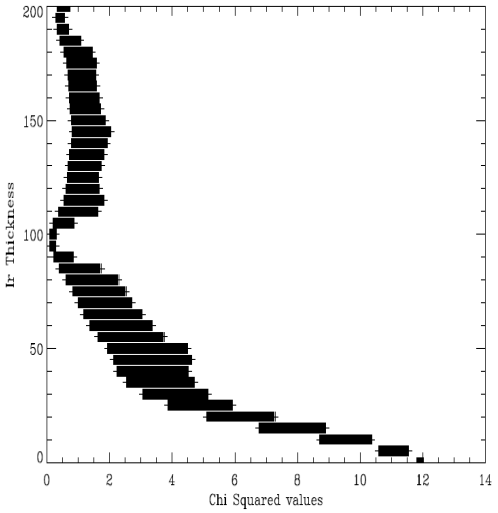

(a) Sample Si6372 Ir thickness in Å

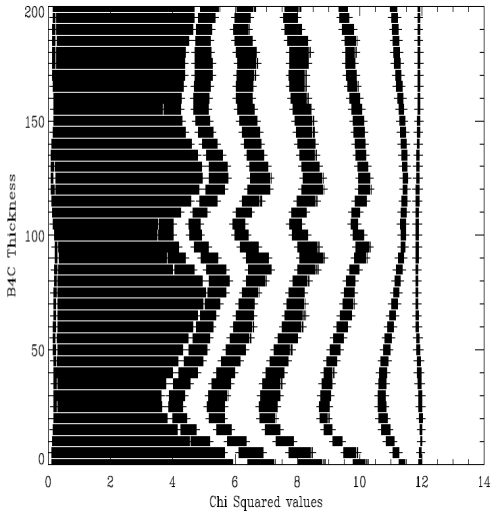

(b) Sample Si6372 B_4C thickness in Å

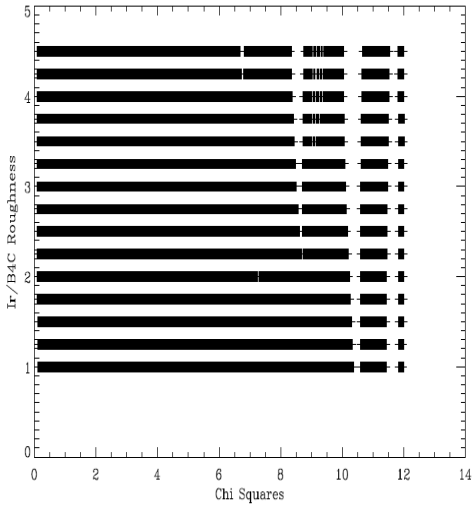

(c) Sample Si6372 Ir/B_4C roughness in Å

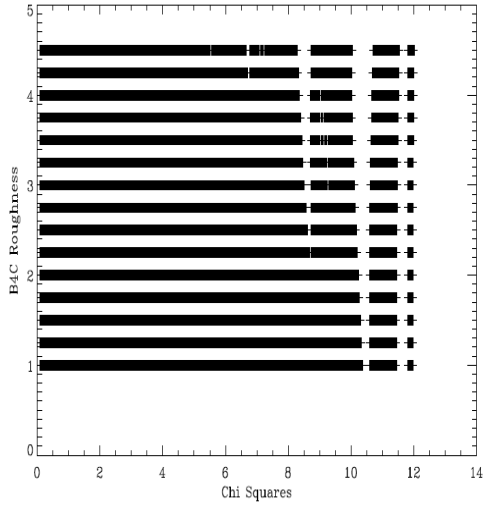

(d) Sample Si6372 B_4C roughness in Å

Figure 5.11: Chi-Square plots without footprint, sample Si6372

Removing the data effected by footprint, gives the following values for each parameter:

- B_4C thickness = 130 Å
- B_4C roughness = 2 Å
- Ir thickness = 100 Å
- Ir/B_4C roughness = 3.5 Å

Observing figure 5.11, the only variable which is visually constrained is the iridium thickness. The B_4C thickness has a tendency to curve in the interval 100-150 Å, which could indicate some form of constrainment, but not enough for any determination. The roughness for both layers are not visually constrained and has no sign of it. Therefor it is not possible to make any assumptions on the B_4C thickness, Ir/B_4C interface and B_4C roughness. Since the iridium is able to be constrained at 100 Å for both with and without data effected by the footprint, it is assumed that the coated thickness is equal to the expected. The 8 keV source and the properties of B_4C, could be the reason that it is not able to be observed. Therefor it is assumed that B_4C has a thickness equal to the expected. Thus, the B_4C layer is locked to its expected values, with a thickness of 80 Å and a roughness of 2.5 Å.

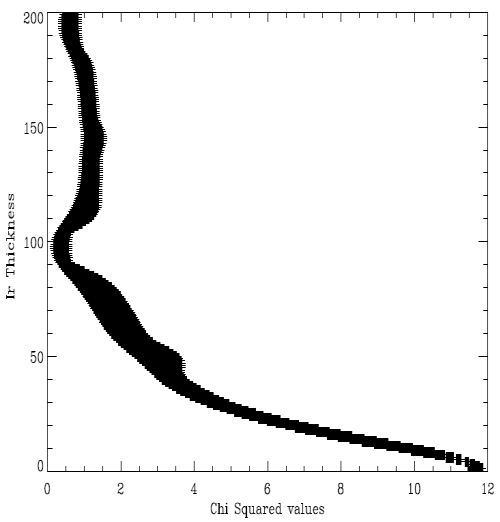

(a) Sample Si6372 Ir thickness in Å

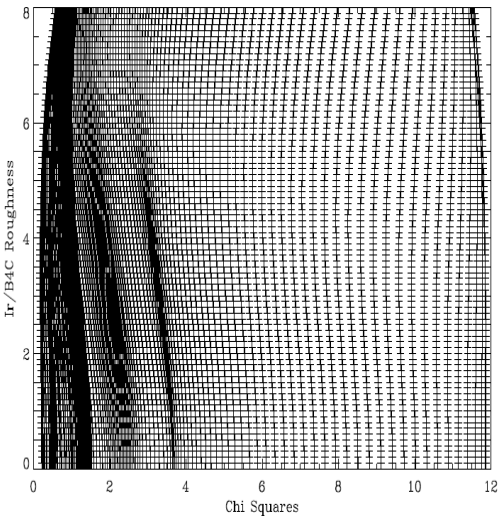

(b) Sample Si6372 Ir/B_4C roughness in Å

Figure 5.12: Chi plots for Sample Si6372 with B_4C thickness and roughness locked on 80 Å and 2.5 Å

Running the IDL script with B_4C locked to 80 Å, the iridium thickness is able to be constrained to a more specific value. Observing figure 5.12a, the iridium thickness is more constrained at 98 Å. The Ir/B_4C interface roughness observed on figure 5.12b, it is not able to be constrained, because it does not converge towards a specific value.
On figure 5.8, $\theta = 3 - 4°$ resembles noise. To test if the noise has any impact on the XRR-data, a measurement is conducted from $\theta = 0 - 10°$.

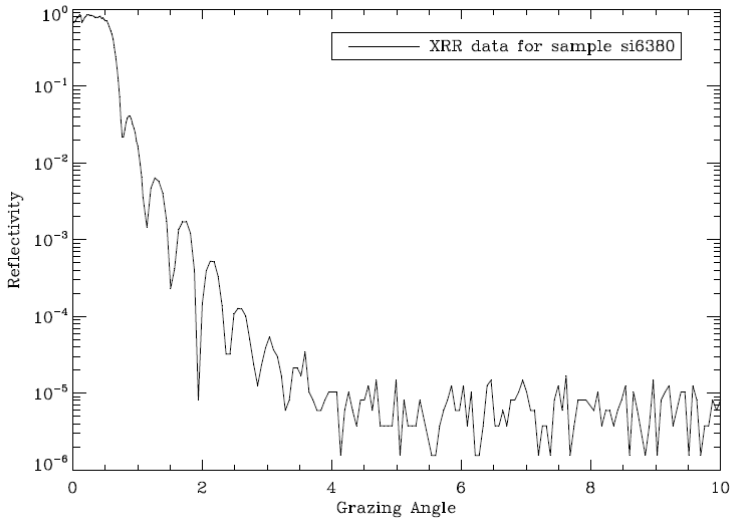

Figure 5.13: Plot showing sample Si6380 going from 0-10°

Observing figure 5.13, the background noise is visible at $\theta = 3°$ and becomes dominant around $\theta = 4°$. The script created for this project does not compensate for the noise, and the data is therefor weighted from $\theta = 0.3 - 2°$.

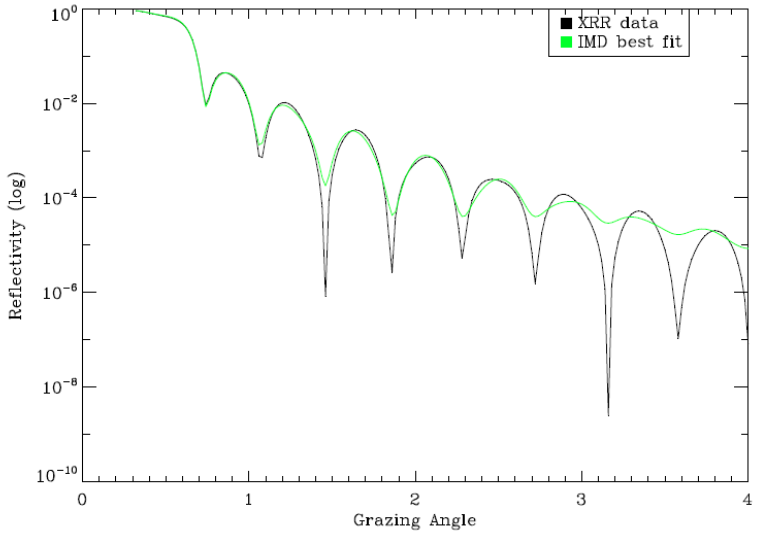

Figure 5.14: Sample Si6372, best IMD fit with weighted values

Comparing figure 5.14 and 5.10, there is a small difference between the two IMD fit. The procedure followed for the non-weighted data is used as well for the weighted data, and figure 5.15 shows the Chi-square plots.

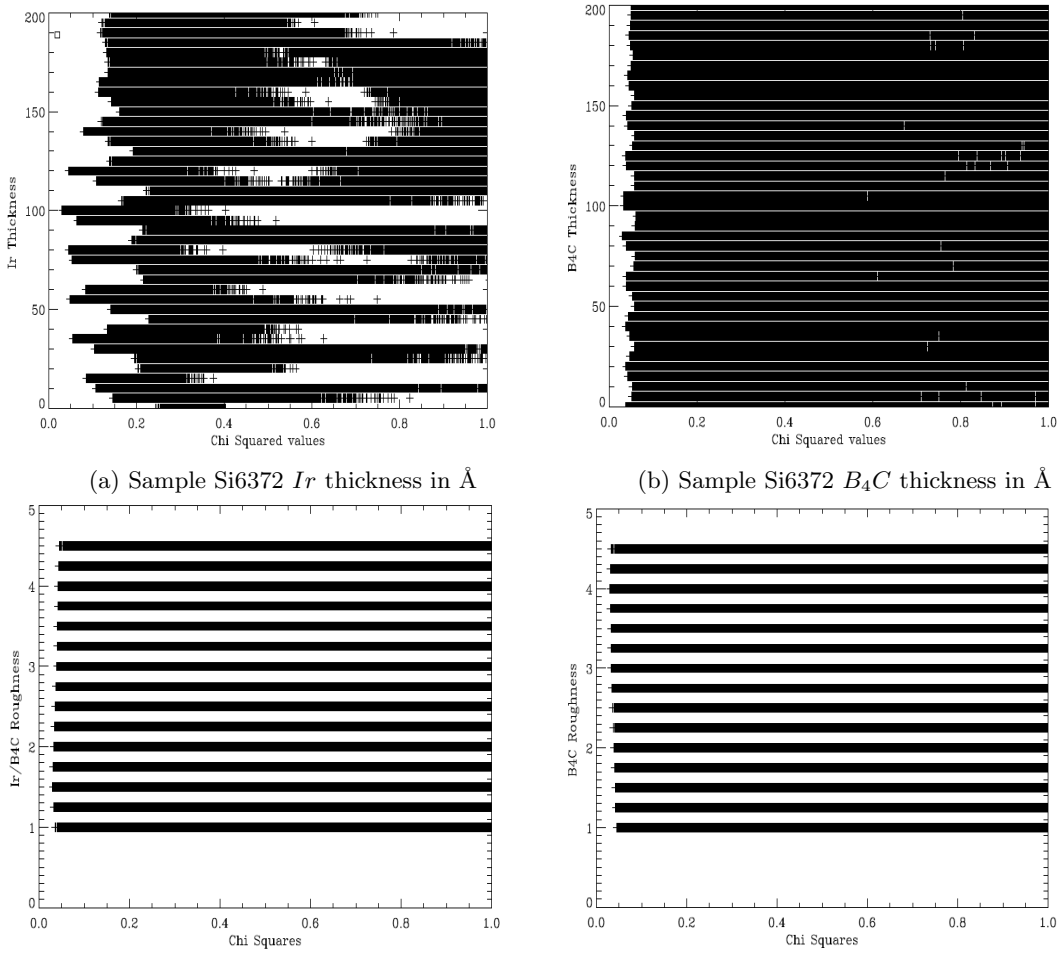

(a) Sample Si6372 Ir thickness in Å

(b) Sample Si6372 B_4C thickness in Å

(c) Sample Si6372 Ir/B_4C roughness in Å

(d) Sample Si6372 B_4C roughness in Å

Figure 5.15: Sample Si6372 with weighted chi-square values

With weighted data, a Chi-square value of $\chi^2 = 0.17$, and the following values for each parameter is:

- B_4C thickness = 85 Å
- B_4C roughness = 4 Å
- Ir thickness = 100 Å
- Ir/B_4C roughness = 1.5 Å

Comparing figure 5.15 and figure 5.11, there is a coherent iridium thickness of 100 Å. Following the same procedure, the B_4C thickness and roughness are locked, to the expected thickness 80 Å and roughness 2.5 Å.

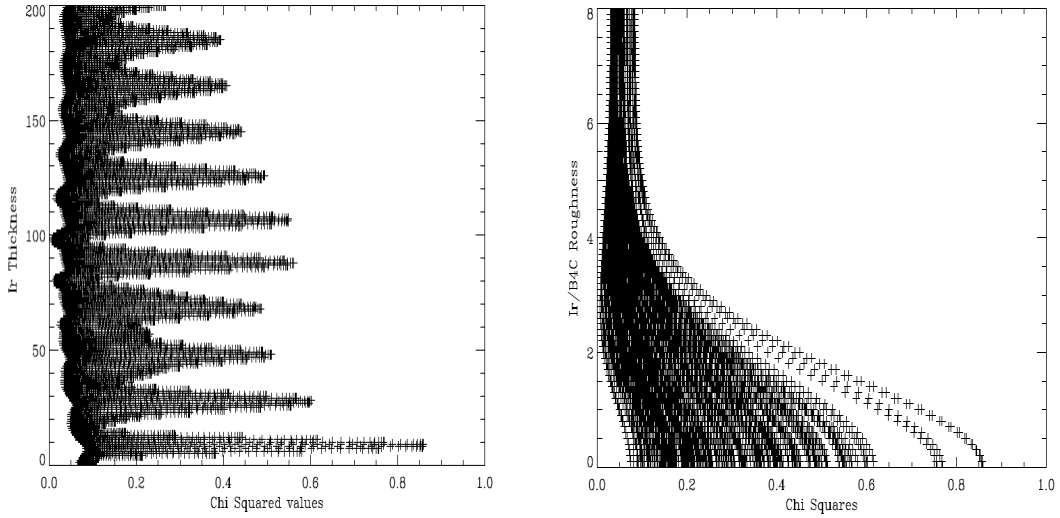

(a) Sample Si6372 Ir thickness in Å

(b) Sample Si6372 Ir/B_4C roughness in Å

Figure 5.16: Chi plots for Sample Si6372 with B_4C thickness and roughness locked on 80 Å and 2.5 Å, weighted values

Figure 5.16 shows the iridium thickness is less constrained, compared to non-weighted figure 5.12. The Ir/B_4C interface roughness on weighted figure 5.16 shows a better constrainment. The iridium thickness on weighted figure 5.16a shows an iridium thickness of 98 Å, which is the same as the non-weighted value. Though the Ir/B_4C interface roughness is more constrained, and is determined to be 2.8 Å. Visually, figure 5.14 has the best fit, but since the calculated Chi-square is lower for the non-weighted model, the weighted model is disregarded. Thus, when it comes to analyzing the data, the non-weighted method is prioritized. Figure 5.17, shows the best IMD fit for the non-weighted and weighted model. It is noticed that the two plots are very similar and the difference is at $\theta = 2 - 4°$.

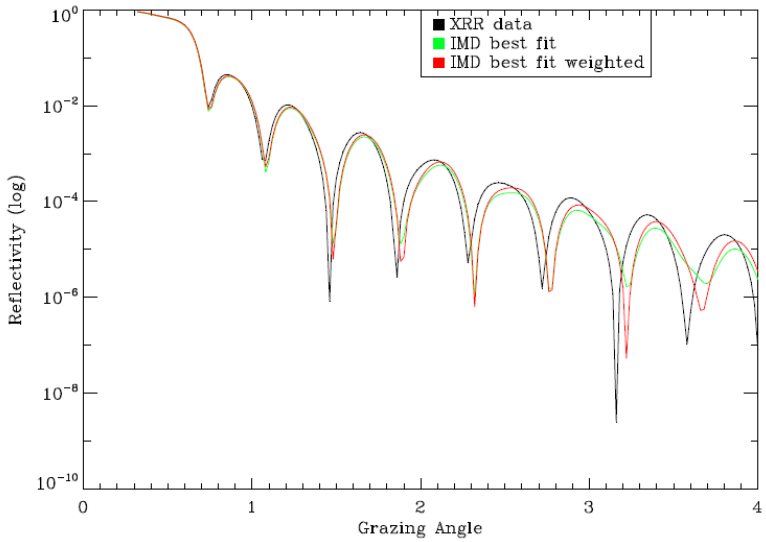

Figure 5.17: Sample Si6372 best IMD fit with non-weighted and weighted values

5.4 Uncertainty on XRR measurements

Multiple XRR measurements have been conducted during the course of the project. Each measurement requires an initial alignment of the sample with respect to the incoming beam. With each alignment, the coordinates thx, thy and th of the sample-holder is aligned. The alignment procedure used for each measurement, is described in the user manual [16]. Furthermore, during the course of the project the detector was replaced with a similar, and the detectors gas-pressure was changed. Figure 5.18 shows 8 XRR measurements for reference sample Si6380, conducted independently throughout the course of the project.

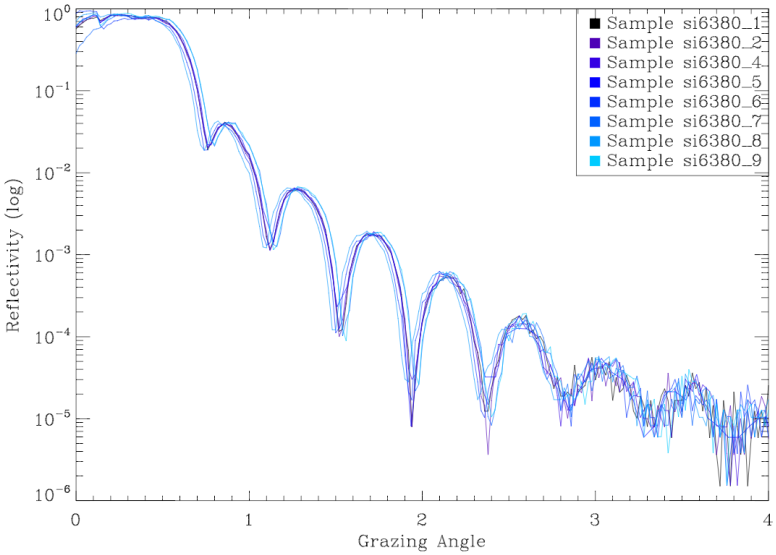

Figure 5.18: 8 XRR measurement, sample Si6380

A variation is noticed in the reflected intensities at grazing angles $\theta = 0 - 0.3$. This is caused by the variation in the alignment of coordinate thx. Grazing angle $\theta = 0 - 0.3$, is as mentioned, where the reflectivity is influenced by the footprint, and can therefor be neglected. Figure 5.18 shows a variation in which grazing angle the Bragg peak is located. This is due the alignment variation in coordinate th. Figure 5.19 shows the 8 XRR measurements for sample Si6380, where the grazing angle is set with an offset of $\theta \sim 0.2$.

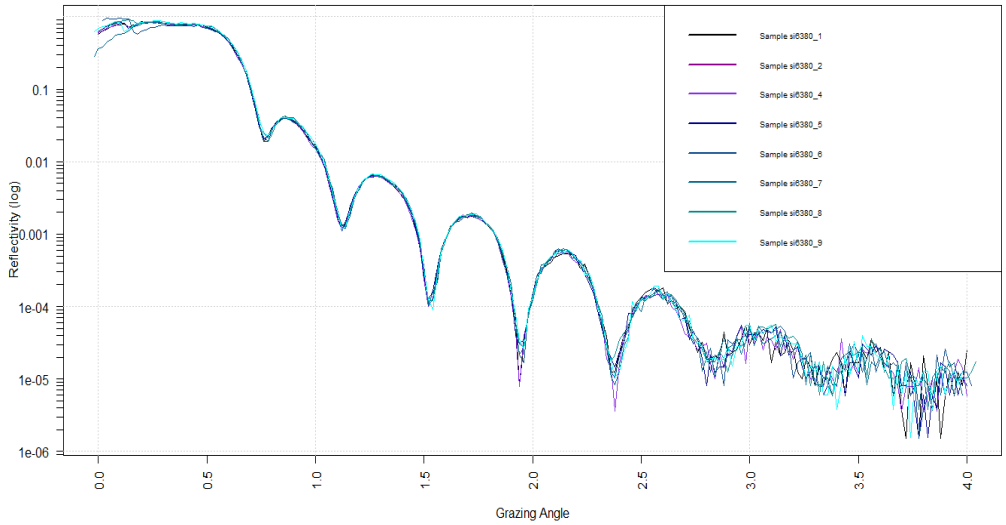

Figure 5.19: 8 XRR measurement with an angle offset, sample Si6380

With an offset of $\theta \sim 0.2$, the Bragg peaks align. Thus the variation in the th alignment has no influence on the measured reflectivity. The standard deviation of the reflected intensity at the first Bragg peak is $\sigma = 0.0012$. This implies that the alignment procedure, replacement of detector and detector gas-pressure, does not effect the amount of measured intensity.

Using the IDL-script and built in Fresnel function, it is possible to determine the Ir thickness and roughness for all samples, by simulating a best fit for the measured XRR data. There is a thickness deviation across all samples, shown on figure 5.20, indicating that the coating is not homogeneous. The sample thickness relies on the position in the coating chamber, and therefor the samples are not coated identically.

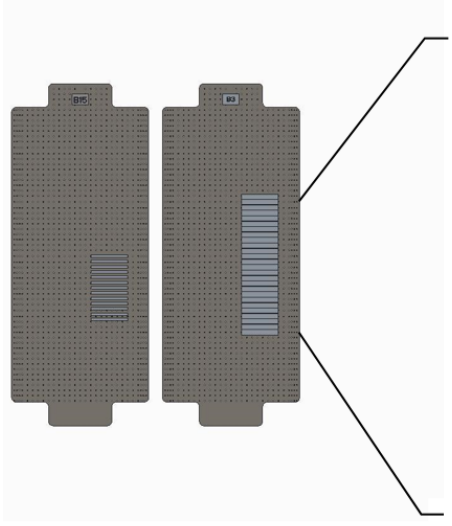

Ir Thickness (Å)	Ir/B_4C Roughness (Å)
93	1.7
94	2.5
94	3.1
90	0.6
92	0
95	1.6
93	0
95	1.9
94	1.8
94	2.3
94	1.4
94	1.2
97	3.7
97	2.1
95	0
98	3.4
96	2.2
97	1.9
97	1.7
97	1.6
-	-
97	2.5
-	-
95	2.7
92	0
92	1.0

Figure 5.20: Left: Plate B15, stress samples S0902-S0914.
Right: Plate B3, witness samples Si6357-Si6382, and corresponding thickness and roughness

6 | Thermal X-ray Reflectivity Measurements

ATHENA uses an annealing procedure for post-stacking the SPO's. This process requires the mirrors to undergo thermal heating up to 200°Celsius for 50 hours, plus 2 hours of preheating. The purpose of thermal test, is to verify if the annealing procedure does any damage to the coating. ESA has made a procedure, which is followed to ensure the same conditions are kept [8]. The vacuum oven, OV-11/12, is used for heating made by, Lab Companion [4]. For each thermal test the oven is cleaned with ethanol, to ensure a clean surface. The samples are placed in the oven, as shown in figure 6.1. The oven is set to 200 °C with an off-timer equal to 50 hours. The oven required two hours to reach a steady temperature of 200°C, which ensured very little variation in temperature. To keep status on the temperature, a computer is connected to the oven. After each test, the samples were kept in the oven until reaching room temperature before removing them. Thermal tests at different temperatures are conducted. After each thermal test XRR- and stress measurements are made to inspect any change in reflectivity and stress.

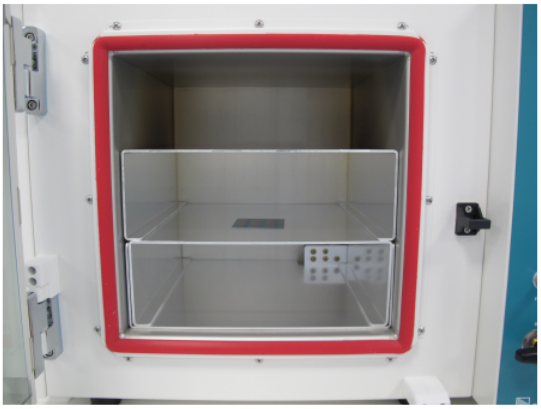

Figure 6.1: Sample in the oven

6.1 Thermal XRR tests

XRR measurements are made after each thermal test, to study any deviation in reflectivity. The previously mentioned IDL-script, shown in appendix **J**, is taken to use for determining the thickness and roughness of each layer. A plot is made containing XRR data from the heated sample and the sample before heating. Sample Si6380 is included in each plot as reference. Figure 6.2 shows sample Si6372, before and after heating at temperature $T = 200^{\circ}$ C.

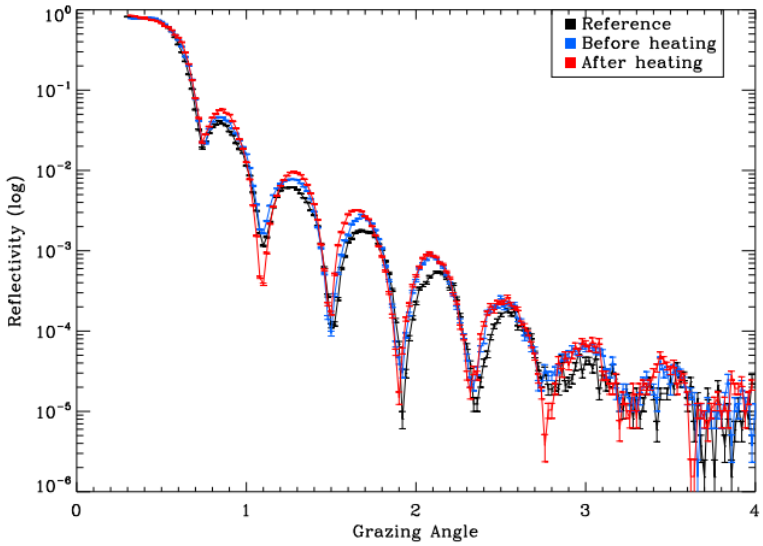

Figure 6.2: Sample Si6372 before and after heating, $T = 200^{\circ}$ C with reference Si6380

It is noticed that the reference curve for sample Si6380, does not match the reflectivity curve for sample Si6372 before heating. It supports the claim of inhomogeneous coating.
Using the IDL-script, the Chi-square values are calculated, and plotted to assist in determining the thickness and roughness of the samples after heating. Observing figure 6.2, there is a small difference in the before and after heating reflectivity curve, indicating that their thickness and roughness are not identical. From the heated sample, the following values of thickness and roughness are given:

- B_4C thickness = 0.0 Å
- Ir thickness = 95 Å
- B_4C roughness = 3 Å
- Ir/B_4C roughness = 1.75 Å

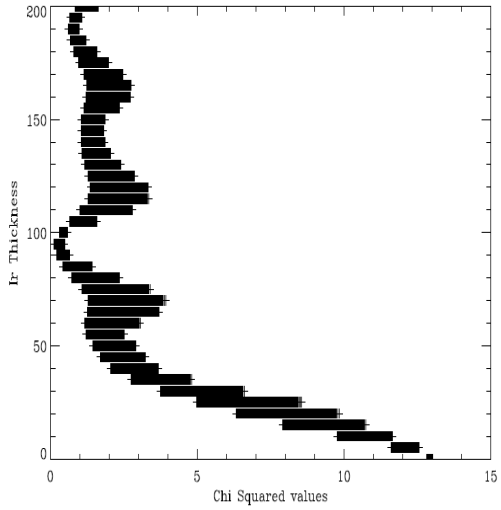

(a) Sample Si6372 heated Ir thickness in Å

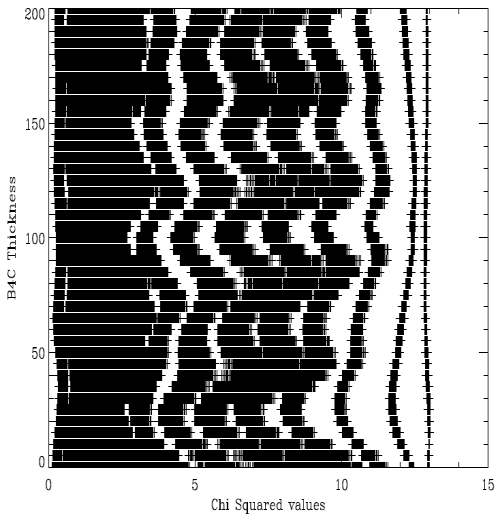

(b) Sample Si6372 heated B_4C thickness in Å

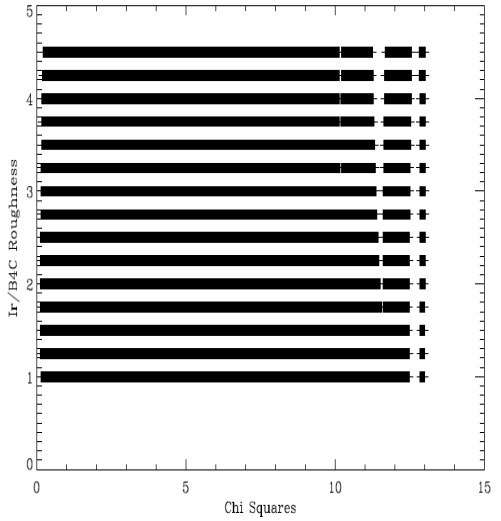

(c) Sample Si6372 heated Ir/B_4C roughness in Å

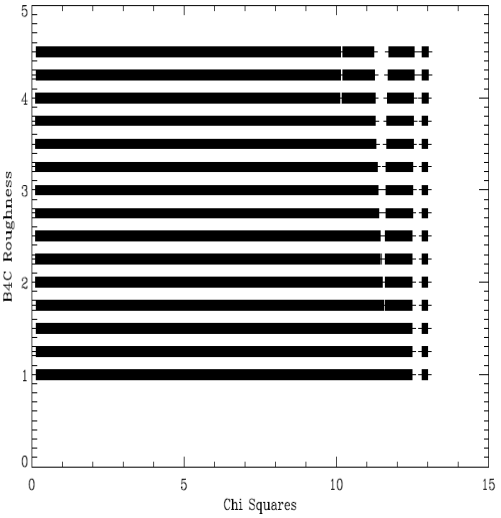

(d) Sample Si6372 heated B_4C roughness in Å

Figure 6.3: Chi-Square plots for sample Si6372 after heating

Observing figure 6.3, the same pattern occurs for the iridium thickness, as to before heating. The B_4C thickness and roughness, and Ir/B_4C interface roughness is not able be constrained. Following the same procedure as to before heating, locking the B_4C thickness and roughness, creates a new Chi-square visual.

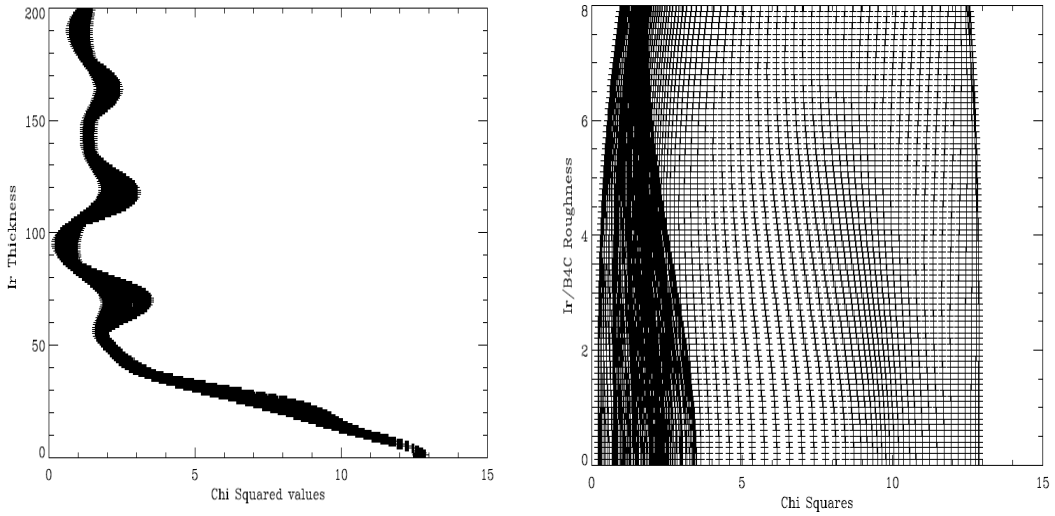

(a) Sample Si6372 heated Ir thickness in Å

(b) Sample Si6372 heated Ir/B_4C roughness in Å

Figure 6.4: Chi-Square plots for sample Si6372 after heating, B_4C locked

The iridium thickness can be constrained to 95 Å, and the Ir/B_4C interface roughness to 1 Å. It is inconclusive to say that the Ir/B_4C interface roughness is 1 Å, because it can not be constrained, compared to the Ir thickness. The Ir thickness, and Ir/B_4C interface roughness has been calculated for all samples, shown in appendix **G**. Comparing the iridium thickness before and after heating, there is a decrease of ~ 2 Å after heating.

6.1.1 Two sample t-test

To test if the annealing procedure has an effect on the amount of X-ray that is reflected at different grazing angles, multiple two-sample t-tests have been conducted using RStudio. A two-sample t-test has been made to compare the means of the same data group, and to test if there is a significant difference between the two data groups. Figure 6.5 shows three XRR measurements before and after heating for sample Si6372.

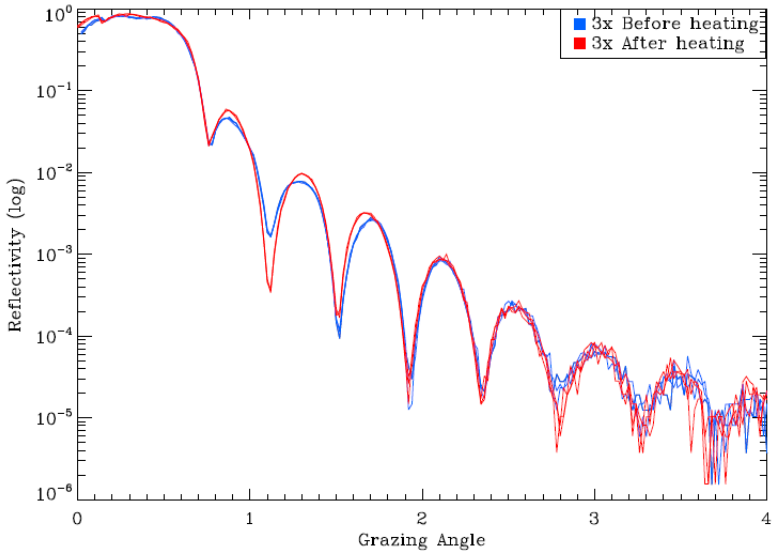

Figure 6.5: XRR before and after heating, Temperature: 200°C, Sample Si6372

The two-sample t-test has been conducted on the XRR measurement for sample

Si6372 before heating (BH). The null hypothesis is that each XRR measurement is identical, and thus the alignment has no effect on the measured reflectivity.

$$\begin{aligned} H_0 &: \mu_{BH} = \mu_{BH} \\ H_1 &: \mu_{BH} \neq \mu_{BH} \end{aligned} \tag{6.1}$$

If the calculated p-value is equal to or less than $\alpha = 0.05$, the null hypothesis is rejected. Figure 6.6 shows the calculated p-values, where the null hypothesis is accepted. It can be concluded that there is no difference between the means, and thus the alignment has no effect on the measured reflectivity.

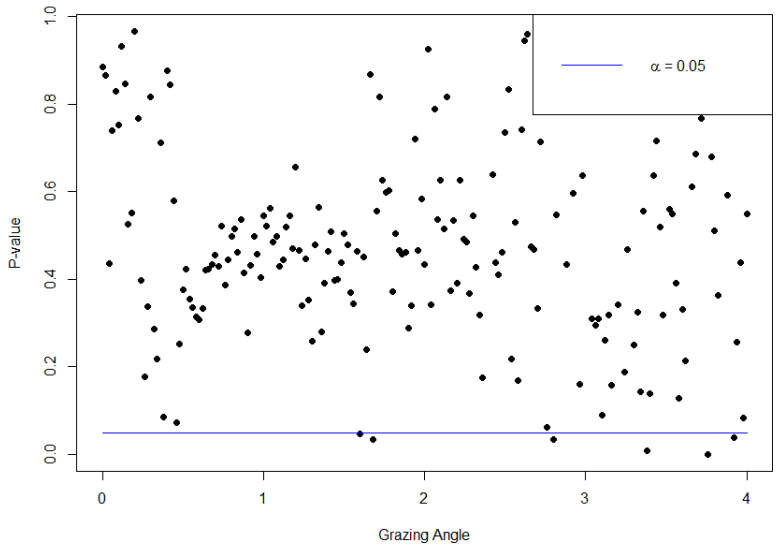

Figure 6.6: Two-sample t-test for same group, before heating, Sample Si6372

A two-sample t-test has been conducted to compare the means of the two groups, before heating (BH) and after heating (AH). The null hypothesis is that the two groups are equal. The alternative hypothesis is that the two groups are different.

$$\begin{aligned} H_0 &: \mu_{BH} = \mu_{AH} \\ H_1 &: \mu_{BH} \neq \mu_{AH} \end{aligned} \tag{6.2}$$

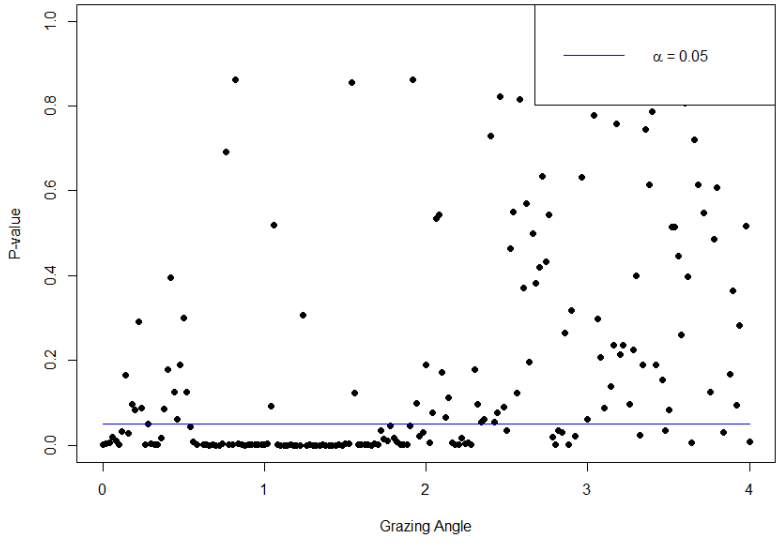

Figure 6.7: Two-sample t-test for two groups, before and after heating, Sample Si6372

Figure 6.7 shows that the means are significantly different between the two groups, for grazing angles $\theta = 0-2.5°$, rejecting the null hypothesis. For grazing angles $\theta > 3°$, there is no significant difference because of the varying noise. This provides a statistical argument that $\mu_{BH} \neq \mu_{AH}$, thus the annealing procedure effects spectral reflectivity.

7 | Stress Measurements

Parallel with the XRR experiment, the curvature of 13 stress samples have been scanned by a Dektak stylus profiler, located in the Multilab. The stress samples are scanned 5.5 cm across the center of the substrate, with a force of 10.00 mg, by a sensitive 50 nm-radius tip needle [21]. They were placed on an engraved platform, to ensure that each measurement was scanned in the same portion of the sample. Scans where made pre-deposition, post-deposition and after heating. To remove dust particles, the samples were polished with pressured air before each measurement, and the platform with a soft brush. Each measurement was conducted with the procedure described in the stress user manual [26].

The sensitive needle measures the height as a continuous function of distance along the sample surface, where the radius of curvature at any given point can be expressed as:

$$R(x) = \frac{(1 + y'^2)^{3/2}}{y''} \tag{7.1}$$

Where $y' = \frac{dy}{dx}$ and $y'' = \frac{d^2y}{dx^2}$.
The stress of the substrate can be calculated with Stoney's equation, using the radius of curvature for the sample:

$$\sigma = \frac{1}{6}(\frac{1}{R_{post}} - \frac{1}{R_{pre}})\frac{E}{1-v}\frac{t_s^2}{t_f} \tag{7.2}$$

A negative stress value corresponds to a compressive stress curvature, where $R_{post} > R_{pre}$. A positive stress value corresponds to a tensile stress curvature, where $R_{post} < R_{pre}$. The Dektak software provides an analytic function, which computes the stress for two measurements using Stoney's equation. Therefore the samples were at minimum scanned twice pre-deposition, post-deposition and after heating. With the two scans, an average stress was calculated, and was to be less than 100 MPa. With Stoney's equation implemented in a Matlab script, appendix **D**, the average stress induced in the substrates after deposition is calculated, shown in table 7.1.

Sample	Stress σ (MPa)
S0902	-1458.2
S0903	-1255.2
S0904	-1145.7
S0905	-1290.5
S0906	-918.2
S0907	-1578.1
S0908	–
S0909	-1527.6
S0910	-1696.1
S0911	-1486.7
S0912	-2865.7
S0913	-1103.5
S0914	-2031.9

Table 7.1: Calculated stress, pre- and post-deposition

Table 7.1 displays that a compressive stress has been induced in the samples due deposition. This is expected since $R_{post} > R_{pre}$, because of the deposited thin film. The previous discussed XRR measurements showed that the thickness of the deposited coating is not homogeneous throughout the coating plate, which would also give rise to different magnitudes of induced compressive stress. Due to the amount of coated stress samples, and their width, they were all centered in front of the sputtering cathode. It is thus assumed that the stress samples have a reasonably even thickness. Therefor all the calculations using Stoney's equation are calculated with a film thickness $t_f = 180$ Å, a substrate thickness $t_s = 0.5$ mm, and a constant elasticity $\frac{E}{1-v} = 1.805 \cdot 10^{11}$ dyne/cm^2.

The samples have a mean compressive stress of $\mu = -1529.8$ MPa, with a standard deviation of $\sigma = 514.31$ MPa. Stoney's equation assumes an initial flat substrate [21].

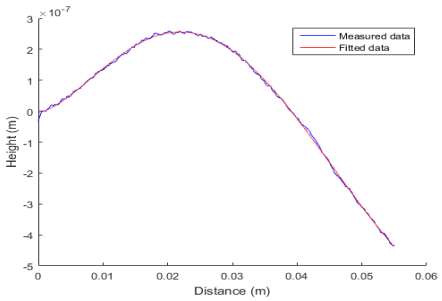

(a) Curvature as a function of distance, Sample S0903

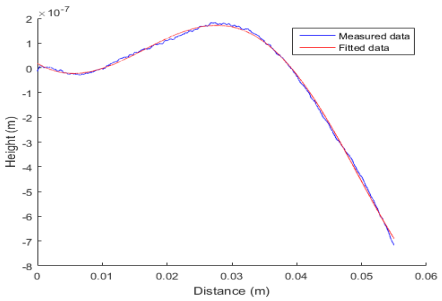

(b) Curvature as a function of distance, Sample S0904

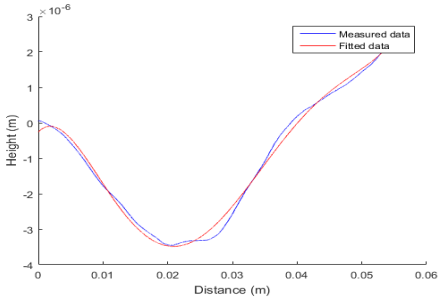

(c) Curvature as a function of distance, Sample S0907

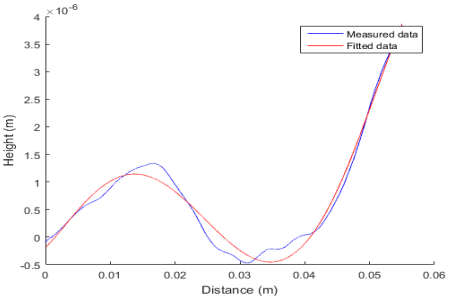

(d) Curvature as a function of distance, Sample S0911

Figure 7.1: Curvature as a function of distance before deposition

Figure 7.1 shows the curvature of sample S0903, S0904, S0907 and S0911 before deposition. Each substrate has an initial curvature, which could cause the deviation in the calculated compressive stress. The goodness of the fit depends on the fluctuation in the substrates curvature, since the fitted model is of a 5^{th} order polynomial of the measured curvature. Appendix **C** fig. 13.1 shows the curvature as a function of distance before deposition for all samples, and appendix **C** fig. 13.3 for all after deposition.

The mean surface curvature for the samples before deposition is $\mu \sim -1350$ Å, with a standard deviation $\sigma_{sd} \sim 5240$ Å. The mean surface curvature for the samples after deposition is $\mu \sim 425$ Å, with standard deviation $\sigma_{sd} \sim 4206$ Å. The surface curvature has thus on average flattened due reflective thin film deposition.

7.1 Thermal Stress Measurements

The stress samples have undergone thermals tests for the purpose of detecting any deformation in the curvature, as an effect of the annealing procedure. The thermal procedure for the stress samples are the same as of the witness samples, described in section 6. All stress samples are scanned after thermal tests, with the same procedure as for pre- and post-deposition. Due time limitations, thermal tests were made for 6 of the 13 stress samples. Appendix **C** fig. 13.5 shows the curvature as a function of distance after heating. The stress induced in the substrates after heating, σ_T, is calculated and shown in table 7.2, including the stress induced after deposition σ:

Sample	Stress σ (MPa)	Temperature (°C)	Stress σ_T (MPa)
S0902	−1458.2	50	−820.8
S0903	−1255.2	200	330.4
S0904	−1145.7	100	−53.8
S0905	−1219.0	150	158.2
S0906	−918.2	–	–
S0907	−1578.1	50	−915.3
S0908	–	–	–
S0909	−1527.6	–	–
S0910	−1696.1	–	–
S0911	−1486.7	75	−596.7
S0912	−2865.7	–	–
S0913	−1103.5	–	–
S0914	−2031.9	–	–

Table 7.2: Calculated stress, σ (pre- and post-deposition), σ_T (pre-deposition and after heating)

The stress induced in the samples have been calculated using Stoney's equation, where R_{pre} is the radius of curvature before deposition, and R_{post} is the radius of curvature after heating, dedicated R_T. Figure 7.2 shows the relative changes in stress $(-\frac{\sigma_T - \sigma}{\sigma})$ as a function of temperature.

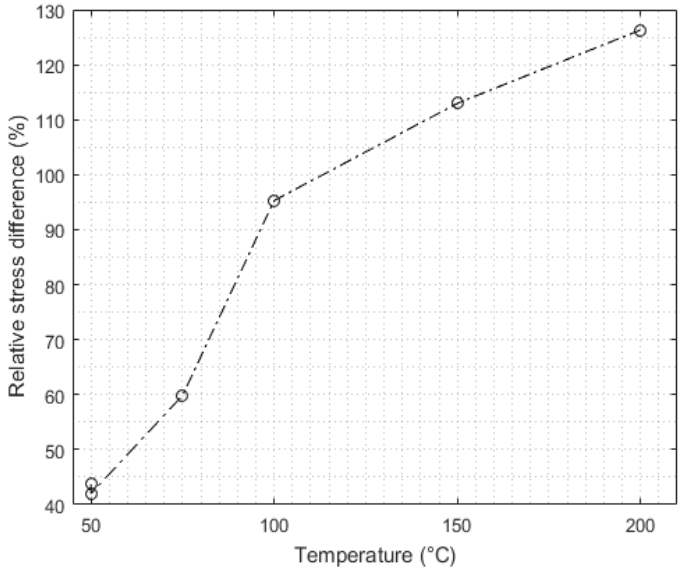

Figure 7.2: Relative changes in stress as a function of temperature

From $T = 50 - 100$°C, the stress induced as a result of deposition, is significantly

reduced. At $T = 100$°C relative stress difference is $\sim 100\%$, with a compressive stress $\sigma_T = -53.8$ MPa, thus the stress induced as a result of deposition is canceled. With a higher temperature $T > 100$°C, the compressive stress is transitioned, where a tensile stress is induced in the sample.
Appendix **C** fig. 13.6 shows the mean height before deposition, after deposition and after heating. It is noticed that there is a coherent change in the measured height, depending on the annealing temperature. After temperatures $T > 100$°C, the mean height of the sample is lower than the initial height, which explains the induced tensile stress. This suggests that the thermal treatment $T > 100$°C, improves the surface roughness of the sample.

8 | Results and Discussion

When heat is added to a system, the particles gain energy and vibrate faster, forcing each other apart, resulting in an expansion. For the post-stacking process of the SPO's, in the ATHENA mission, the mirrors are heated up to 200°C for 50 hours. Throughout this project, multiple thermal tests have been conducted with different temperatures. All of these measurements are made to study the effect of thermal heating. Appendix **H** includes plots for all the samples that have undergone thermal tests. Each plot includes the reference sample, Si6380, and the respective sample before and after heating. The baseline coating used for ATHENA is Ir/B_4C, which both have a melting point over 2000°C. Boron carbide is one of the hardest materials known, and has hard durability, and iridium is known to be a corrosion-resistant material at high temperatures.
Observing figure 18.1 and figure 18.2 in appendix **H**, there is no consistent change in the measured reflectivity at temperatures $T = 50 - 150^\circ$ C. Investigating the plots for $T = 200^\circ$ C, shown in appendix **H**, figure 18.2, there is a tendency for the reflectivity to increase at the first Bragg peak. Table 8.1 shows the 4 samples relative reflectance difference, when heated up to 200°C.

Sample	Ref_{BH}	Ref_{AH}	Bragg peak, n
Si6372	0.047	0.058	1
Si6375	0.049	0.056	1
Si6376	0.0089	0.010	2
Si6378	0.047	0.052	1

Table 8.1: Relative reflectance difference, 72, 75, 78 for first Bragg peak, 76 for second Bragg peak

Figure 8.1 shows the heated samples relative reflectance difference in %. Sample Si6372, -75 and -78 show a relative increase in reflectivity, at the first Bragg peak. Sample Si6376 has no significant change in reflectivity at the first Bragg peak, though a difference is observed at the second. Figure 8.1 shows the relative reflectance for all the heated samples at their respected temperature. The most conspicuous is that there is an increase in reflectivity after thermal heating at $T = 100^\circ$ C, and again at $T = 200^\circ$ C. This verifies that the thermal procedure has an effect on the coating.

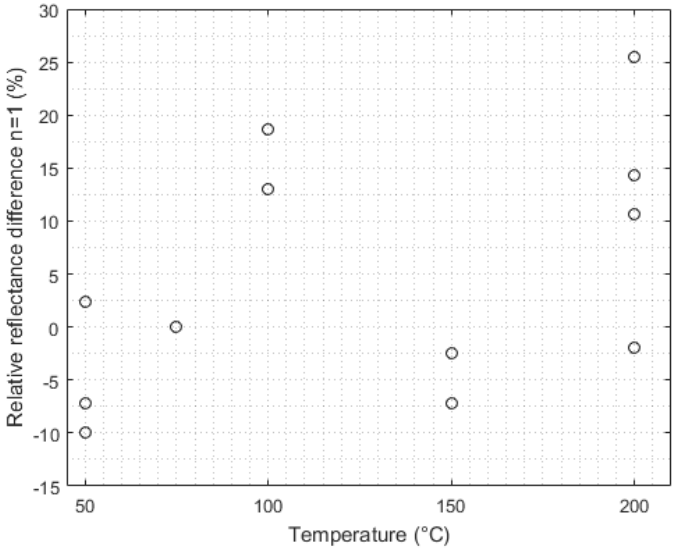

Figure 8.1: Relative reflectance difference for Bragg peak n=1

In section 5.3, it was proven that iridium could be constrained. Table 17.1, in appendix **G**, shows the iridium thickness and Ir/B_4C interface roughness, before and after heating. It is noticed that the iridium thickness decreases with ~ 2 Å for $T = 200°$ C, which doesn't comply with iridium's corrosion-resistance and melting point.

With the IDL-script, is was previously shown that the iridium thickness is able to be constrained, and converges to a specific value. The iridium thickness is locked to its designated value, shown in appendix **G**, and a new simulation is done to assist the constrainment of B_4C. Figure 8.2 shows the calculated Chi-square values for sample Si6360 and Si6372.

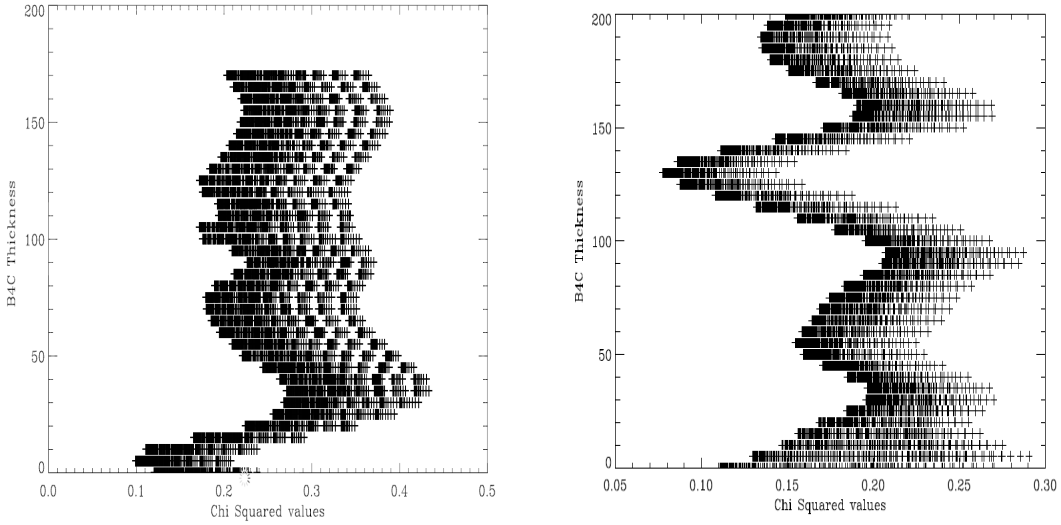

(a) B_4C thickness, sample Si6360

(b) B_4C thickness, sample Si6372

Figure 8.2: Different constrained thicknesses

Figure 8.2 shows both samples to be constrained. Sample Si6360 has a B_4C thickness 5 Å, where as sample Si6372 has a thickness 130 Å. Compared to the iridium thickness, which deviates with a thickness $\sim$2 Å, the B_4C thickness deviation should not be due to the in-homogeneous coating.

Referring to section 2.1, the capabilities of ATHENA's coating was discussed. On figure 2.1, it is noticed that B_4C reflects low energies, and iridium is the dominant material after 3 keV. The XRR measurements were made with an 8 keV source, and hence it should not be possible to observe the B_4C layer. XRR simulations made using the IMD interface for 8, 4 and 1 keV, and are displayed on figure 8.3.

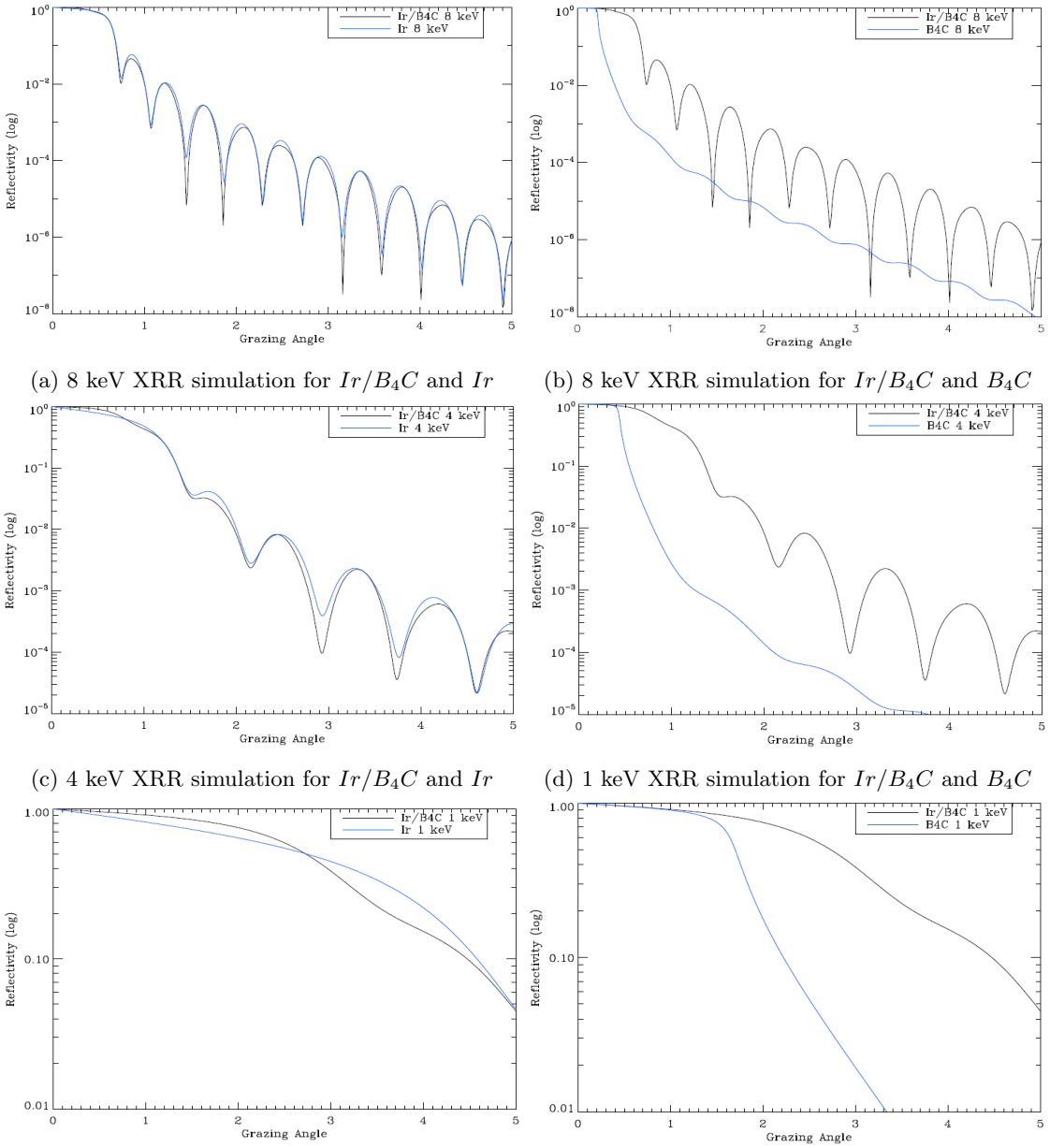

(a) 8 keV XRR simulation for Ir/B_4C and Ir

(b) 8 keV XRR simulation for Ir/B_4C and B_4C

(c) 4 keV XRR simulation for Ir/B_4C and Ir

(d) 1 keV XRR simulation for Ir/B_4C and B_4C

(e) 1 keV XRR simulation for Ir/B_4C and Ir

(f) 1 keV XRR simulation for Ir/B_4C and B_4C

Figure 8.3: IMD interface XRR simulation at 8, 4 and 1 keV for Ir/B_4C, Ir and B_4C, $z_{Ir} = 100$ Å, $z_{B_4C} = 80$ Å

The XRR simulations are made for Ir/B_4C, Ir and B_4C, at different energies, to compare their reflective capabilities. The B_4C is transparent at 8 keV, where as at lower energies B_4C becomes visible. Figure 8.3a shows that at 8 keV, the Ir/B_4C bi-layer and single layer Ir are shown to be very similar, which indicates that the XRR facility at the DTU Space Institute has limitations for measuring B_4C. This verifies the constrained Ir thickness, compared to the varying B_4C. The annealing procedure improves the amount of X-ray reflected at 8 keV. However, the increase in reflectivity could indicate a change in the B_4C layer, since less X-ray is absorbed

by the B_4C layer, and thus more reaches the iridium layer. The deviation for the iridium thickness is relatively small, which might well be on the grounds of an uncertainty. It is interesting that the iridium thickness decreases after a thermal exposure, since heat added to a system should result to an expansion.

8.1 Cumulative heating

A cumulative thermal process has been conducted on sample Si6373 and Si6374. The X-ray reflectivity is measured initially and after each thermal test. The cumulative thermal procedure is of the same thermal process described in sec. 6, where the temperature is increased with 25°C for each iteration. The cumulative XRR measurements for temperatures 50, 100, 150 and 200 °C are shown in Appendix **H** fig. 18.3. Figure 8.4 shows the relative difference in reflection for the first Bragg peak, for all temperatures.

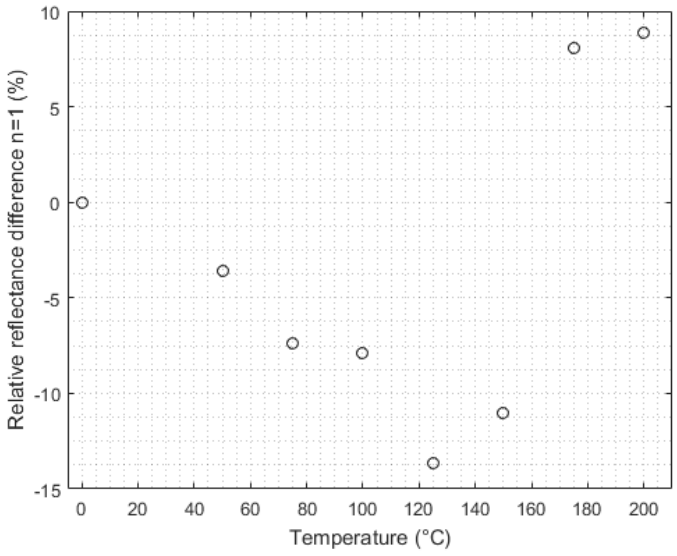

Figure 8.4: Relative reflectance difference for Bragg peak n=1

For temperatures $T <= 150$°C, the reflection is gradually decreased, and for $T > 150$°C the reflection is increased. Figure 8.1 showed that for temperatures $T = 100$°C, the reflectance had increased with $\sim 15\%$, whereas the cumulative reflectance shows a decrease with $\sim 7\%$. This indicates that the cumulative thermal exposure still effects the amount of measured reflectivity, though the cumulative thermal process has a different effect than the standard thermal process.

8.2 Stress

The thermal treatment reduces the stress induced in the samples, thus changing the curvature. At temperatures $T = 100$°C, the radius of curvature after heating is equal to the radius of curvature before deposition, $R_T = R_{pre}$. At temperatures $T > 100$°C the stress becomes tensile $R_T < R_{pre}$. Appendix **C** fig. 13.6, shows that the mean height of the sample at $T = 200^{\circ}$ C, is lower than the initial height, which explains the induced tensile stress, though it is unclear of what layers are effected by the thermal procedure.

Appendix **C** fig. 13.5a shows multiple scans of sample S0902's curvature, after a thermal treatment of 50°C. Stress samples who have undergone thermal tests at temperature $T = 50$°C, shows an average stress values $<<$ 100 MPa, on the Dektak software, when compared with a previous scan. The scans where inconsistent,

as if the surface was flexible. The 50 nm-radius tip needle on the Dektak stylus profiler is very sensitive, and it is unclear if it has been adjusted to a position compromising each scan.

Due the initial substrate roughness, the coated samples will reflect with a diffuse reflection. Figure 7.2 shows that at temperature $T = 100^\circ$ C degrees, the stress induced as a result of deposition is canceled. This could explain the small increase of reflectivity at temperature $T = 100^\circ$ C shown in appendix **H**. Appendix **C** fig. 13.6 shows the mean height after heating is lower than of the initial height, indicating a more flat surface. This results in a less diffuse reflection, thus increasing the amount of measured reflectivity for temperatures $T = 200^\circ$ C.

With the limitations of the equipment, it is inconclusive if the increased reflectivity is caused by a change in the bi-layer thickness, or the decreased stress.

9 | Conclusion

In this project we have evaluated the annealing procedure, done by the European Space Agency at Cosine Research B.V, regarding what effects the annealing procedure will have on the robustness of the ATHENA coating. To replicate the ATHENA coating, silicon substrates were coated with a single Ir/B_4C bi-layer. To test the effects of the thermal heating, stress and X-ray reflectivity measurements have been conducted at DTU's space institute. The XRR measurements are made with an 8 keV X-ray source, and the stress is calculated using the measured curvature scanned by a Dektak stylus profiler. The following conclusions are made from results presented in this paper.

Using the IDL-script with the built in Fresnel function, it is possible to determine the thickness and roughness, by simulating a best fit for the measured XRR data. We can conclude with the available equipment and setup, that it is possible to detect the iridium layer. The iridium thickness converges towards a specific value and can thus be constrained, whereas B_4C is able to be constrained, but the calculated thickness's are inconsistent. It can be concluded that B_4C is transparent at 8 keV, and it is not sufficient to draw any conclusions on these calculated parameters. Chi-square tests are calculated to visualize and improve the determined thickness and roughness. Removing the XRR data which is effected by the X-ray sources footprint, resulted in a better IMD fit. With the two-sample t-test, we can conclude that the XRR measurements have minimal uncertainties, where the alignment has no effect on the measured reflectively.

The X-ray facility is limited in grazing angles $\theta > 4°$, where background-noise becomes dominant, thus the reflectivity was measured in the interval 0-4°. It can be concluded that weighting the XRR data from $\theta = 0.3 - 2°$, the calculated Chi-square value is higher than the non-weighted. Hence it is sufficient to study the non-weighted models.

All samples used in this project have undergone XRR measurements, and the thickness is determined. There is a thickness deviation across all samples before heating, and it can thus be concluded that the coating chamber does not have a homogeneous coating.

We can conclude that the thermal test does not effect the iridium thickness, since it is relatively similar to before heating. There is a deviation across the interval of temperatures, where at 200°C there is an average increase of reflectivity by $\sim 15\%$.

It can be concluded that the coating induces a compressive stress on the substrate. The thermal treatment has a variation in the magnitude of induced stress, across the interval of temperatures. For temperatures $T < 50°C$, the induced stress is decreased. At the temperature $T = 100°C$, the radius of curvature after heating is equal to the radius of curvature before deposition, $R_T = R_{pre}$. At temperatures $T > 100°C$ the mean height of the sample is decreased relative to the initial $R_T < R_{pre}$, so a tensile stress is induced.

From the previous conclusions, we can conclude that the annealing procedure, done by the European Space Agency at Cosine Research B.V, has an effect on the robustness of the ATHENA coating. The annealing procedure has an improvement in the amount of X-ray reflected, where it is concluded that the iridium

thickness shows no significant change. The stress induced due deposition is relatively reduced, but it is not sufficient to draw any conclusion about what layers are effected by the thermal procedure.

9.1 Further Studies

For further studies, other techniques can be used to investigate what affects the thermal process has on the coating. A transmission electron microscope (TEM) is able to take detailed images of the internal micro-structural, with magnifications up to 1.000.000 times. Another useful tool, for investigating the surface of a sample, is the scanning electron microscope (SEM). The image represents the surface features of the sample. To study the changes due to heating, an X-ray photoelectron spectroscopy (XPS) technique can be used to analyze the surface composition. XRR and stress measurements can be conducted on multilayer coated thin film, so a change in the microstructure would be more noticeable. Furthermore, XRR measurements at low energies can be conducted, which would show potential changes in the B_4C structure.

10 | Reference

References

[1] Bragg's law. https://en.wikipedia.org/wiki/Braggs_law. [Retrieved March 25th 2017].

[2] Diffuse reflection figure. http://keywordsuggest.org/gallery/856973.html. [Retrieved March 28th 2017].

[3] Good diffraction practice webinar series. https://www.bruker.com/fileadmin/user_upload/8-PDF-Docs/X-rayDiffraction_ElementalAnalysis/XRD/Webinars/Bruker_AXS_Good_Diffraction_Practice_I_-_X-ray_Reflectometry.pdf.

[4] Lab companion website. http://www.jeiotech.com/eng/index.php.

[5] Roughness effects on thin film physical properties. https://www.rug.nl/staff/g.palasantzas/nanoscale_roughness.pdf. [Retrieved March 25th 2017].

[6] Anders C. Jakobsen, Desiree Della Monica Ferreira, Finn E. Christensen, Brian Shortt, Max Collon, Marcelo D. Ackermann. *Preliminary coating design and coating developments for ATHENA*.

[7] Max Collon Boris Landgraf and David Girou. *Post-stacking annealing of silicon pore optics*. cosine Research B.V., 2017.

[8] Boris Landgraf, Max Collon, David Girou. *Post-stacking annealing of silicon pore optics*.

[9] Martin Chaplin. Hydroxide ions. http://www1.lsbu.ac.uk/water/ionisoh.html, 2008. [Retrieved March 4th 2017].

[10] Germain Chartier. *Introduction to Optics*. Springer Science+Business Media, Inc, manuel d'optique. english edition, 2005.

[11] Collon, Maximilien J.; Vacanti, Giuseppe; Guenther, Ramses; Christensen, Finn Erland. *Silicon Pore Optics development for ATHENA*. Proceedings of SPIE, 2015.

[12] David J. Griffiths. *Electromagnetism for physicists*. Pearson Education Inc., fourth edition, 2015.

[13] ESA. ATHENA to study the hot and energetic universe. http://sci.esa.int/cosmic-vision/54241-athena-to-study-the-hot-and-energetic-universe/, 2017. [Retrieved March 4th 2017].

[14] Desiree Della Monica Ferreira, Finn Erland Christensen, Anders Clemen Jakobsen, Niels Jørgen Stenfeldt Westergaard, and Brian Shortt. Athena optimized coating design. *Proceedings of SPIE, the International Society for Optical Engineering*, 8443:84435L, 2012. Poster Session: Athena.

[15] Desiree Della Monica Ferreira, Finn Erland Christensen, Anders Clemen Jakobsen, Niels Jørgen Stenfeldt Westergaard, and Brian Shortt. Coating optimization for the athena+ mission. *Proceedings of SPIE, the International Society for Optical Engineering*, 8861, 2013.

[16] Finn Erland Christensen, Sonny Massahi. *Guide for operating the X-ray Reflectometer.*

[17] Ch. Hollauer. Modeling of thermal oxidation and stress effect. `http://www.iue.tuwien.ac.at/phd/hollauer/node47.html`.
[Retrieved March 25th 2017].

[18] Jens Als-Nielsen, Des McMorrow. *Elements of Modern X-ray Physics.* John Wiley Sons Ltd, 2001.

[19] Lab Companion, JEIO TECH. *Operation manual [Vacuum oven] Model: OV-11/12.*

[20] Laconte, Jean, Flandre, Denis, Raskin, Jean-Pierre. *Micromachined Thin-Film Sensors for SOI-CMOS Co-Integration.* Springer US, 2006.

[21] Mike Zecchino, Time Cunningham. *Thin Film Stress Measurement using Dektak Stylus Profilers.* Vecco Instruments Inc., 2004.

[22] Peter Ramm, James Jian-Qiang Lu, Maaike M. V. *Handbook of Wafer Bonding.* 2010 Elsevier Inc, second edition, 2015.

[23] PhD thesis of Anders Clemen Jakobsen. *X-ray optics in new instruments for astro- and astroparticle physics.* Technical University of Denmark, National Space Institute, 2015.

[24] Q.-Y. Tong and U. Gösele. *A Model of Low-Temperature Wafer Bonding And Its Applications.* The Electrochemical Society, Inc, J. Electrochem. Soc, 1996.

[25] S. Massahia, D.A. Giroua, D.D.M. Ferreiraa, F.E. Christensena, A.C. Jakobsena, B. Shorttb, M. Collonc and B. Landgrafc. *Investigation of Photolithography Process on SPOs for the ATHENA Mission.* Technical University of Denmark, National Space Institute, 2015.

[26] Sonny Massahi, Joan Momberg. *Guide for measuring the curvature of Silicon samples prior and post thin-film deposition.*

[27] V. Masteika, J. Kowal, N. St. J. Braithwaite, and T. Rogers. *A Review of Hydrophilic SiliconWafer Bonding.* ECS Journal of Solid State Science and Technology, 2014.

[28] William D. Callister, David G. Rethwisch. *Materials Science and Engineering.* John Wiley Sons (Asia) Pte Ltd, eigth edition, 2009.

11 | Appendix A

```
############################
##     Ir/B4C Baseline    ##
############################

def baseline_2_plates_ir_b4c '
        coating_start_log
        closevalve
        setflow 1 76.5
        setpower 1 1000
        setpower 2 600
        openflow 1
        openmainflow
        print("Waiting for Ar flow to settle (120 seconds).
\n")
        sleep(120)
        print("Starting coating.\n")
        print("In start position.\n")
        pson 2
        sleep(300)
        mra -180 778
        psoff 2
      print("Move to start position.\n")
        mra 90 10000
        print("In start position.\n")
        pson 1
        sleep(300)
        mra -180 170
        psoff 1
        print("Move to start position.\n")
        mra -90 10000
        print("Coating over.\n")
        closemainflow
        closeflow 1
        openvalve
        coating_stop_log
'
```

Figure 11.1: Single Ir/B_4C bi-layer coating script

```
## B4C single layer 30, 50 A plus 10[ir/b4c]  ##
###############################################
def irb4c1b4c_4_plates '
        coating_start_log
        closevalve
        setflow 1 76.5
        setpower 1 1000
        setpower 2 600
        openflow 1
        openmainflow
        sleep(120)
        print("Starting coating.\n")
        pson 2
        sleep(300)
        mra -90 2474
        mra -90 1540
        psoff 2
        print("Move to start position.\n")
        mra -90 10000
        pson 1
        sleep(300)
        mra -90 833
        mra -180 500
        mra -90 313
        psoff 1
        print("Move to start position.\n")
        mra -90 10000
        for (j=0;j<9;j++){
                        printf("\nStarting layer %g.\n",j+1)
                        pson 2
                        sleep(120)
                        mra -90 2474
                        mra -90 1540
                        psoff 2
                        print("Move to start position.\n")
                        mra 90 10000
                        pson 1
                        sleep(120)
                        mra -90 500
                        mra -90 313
                        psoff 1
                        print("Move to start position.\n")
                        mra -90 10000
        }
        print("Coating over. Closing flow valve.\n")
        closemainflow
        closeflow 1
        openvalve
        coating_stop_log
'
```

Figure 11.2: 10 Ir/B_4C multi-layer coating calibration script

12 | Appendix B

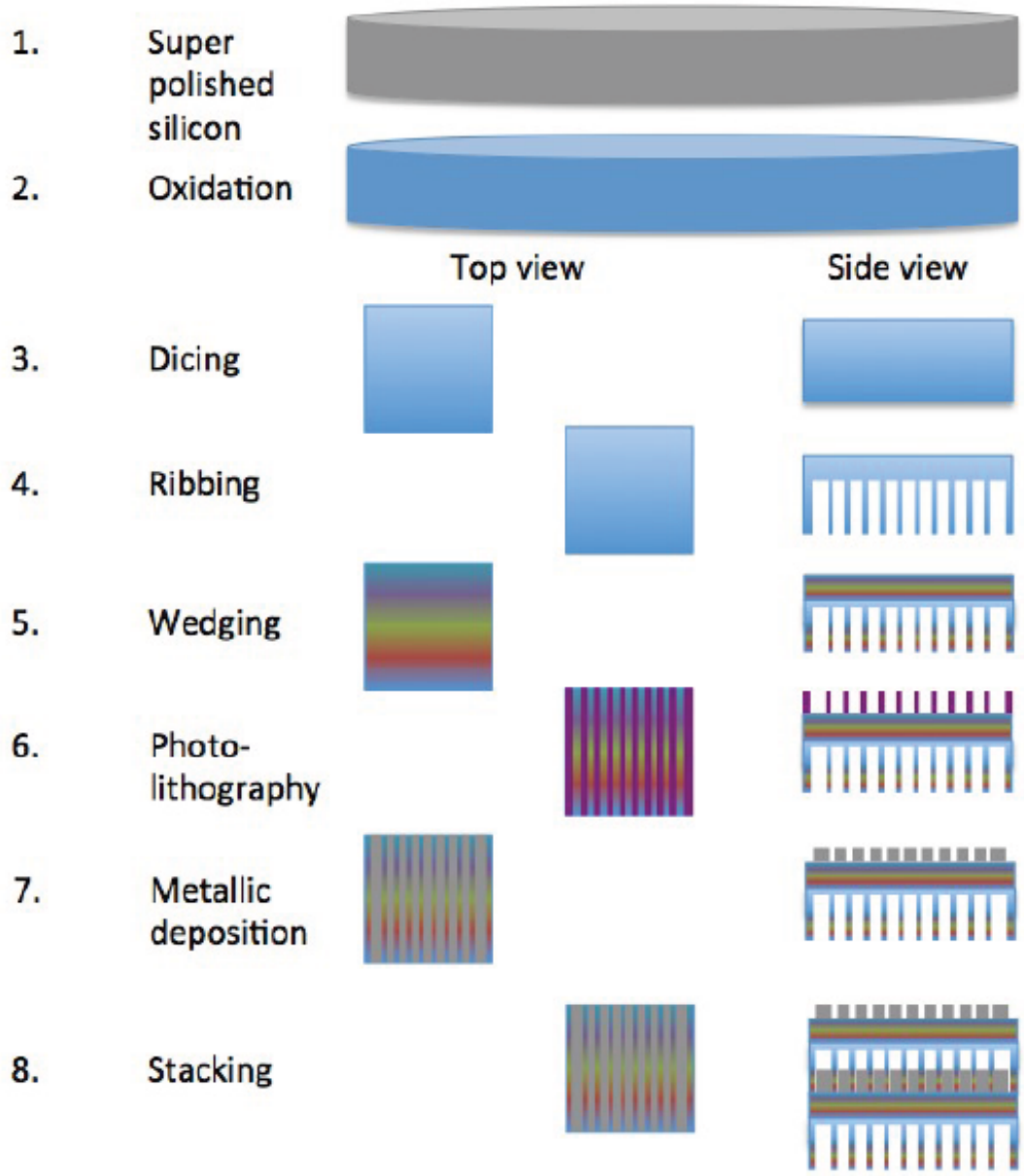

Figure 12.1: Process scheme of the production of an SPO mirror plate and mirror stack [25].

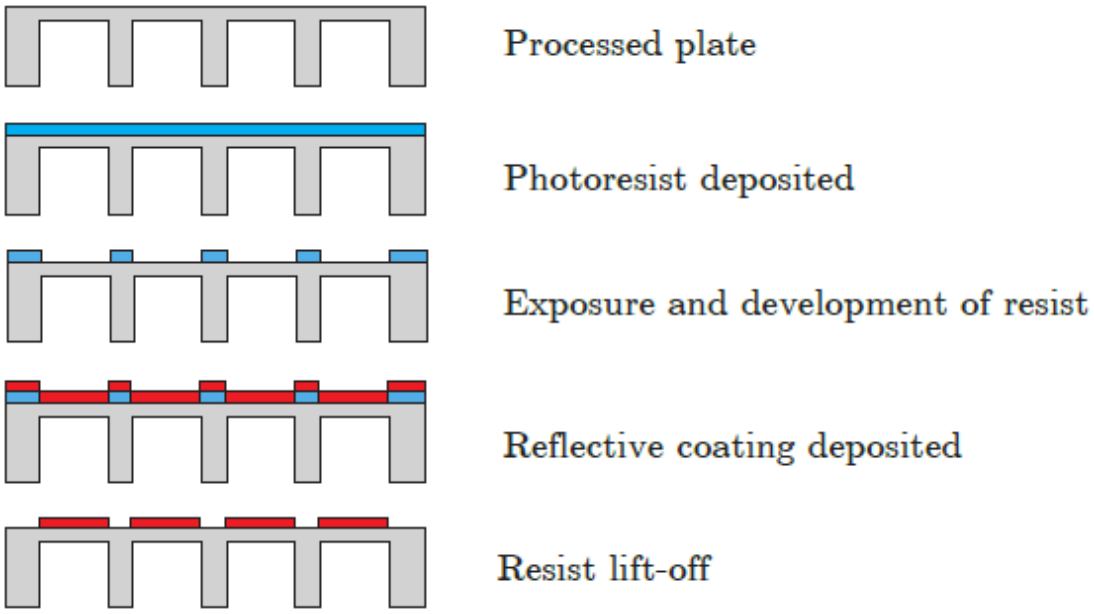

Figure 12.2: The lithographic process applied to SPO substrates to achieve a striped pattern of reflective coating [23].

13 | Appendix C

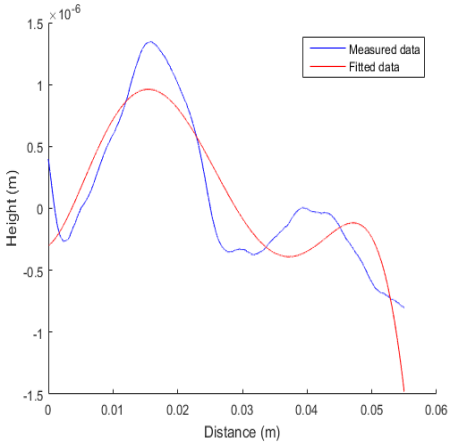

(a) Curvature as a function of distance, Sample S0902

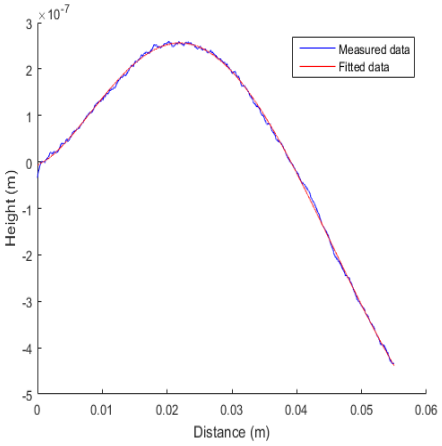

(b) Curvature as a function of distance, Sample S0903

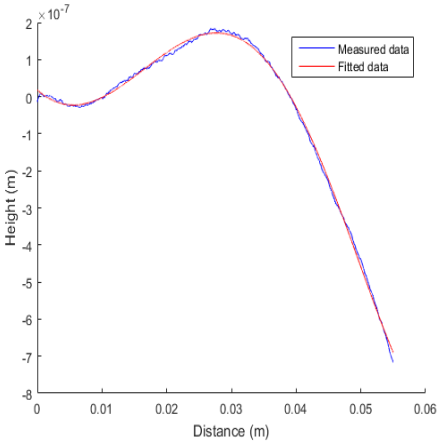

(c) Curvature as a function of distance, Sample S0904

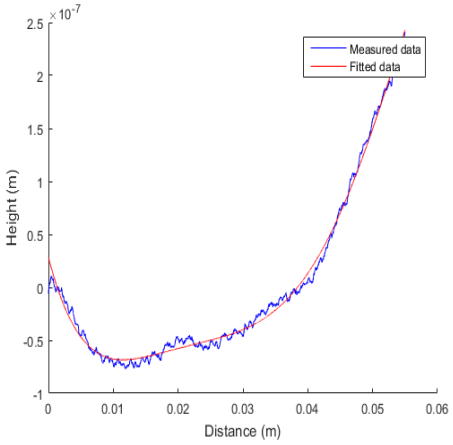

(d) Curvature as a function of distance, Sample S0905

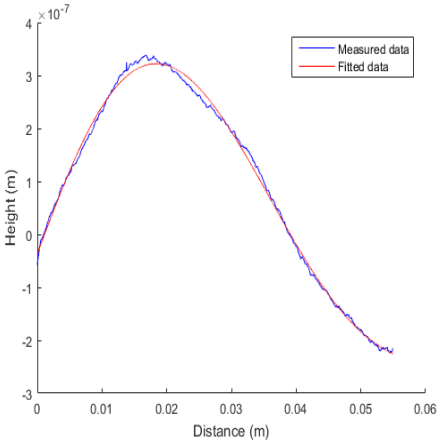

(e) Curvature as a function of distance, Sample S0906

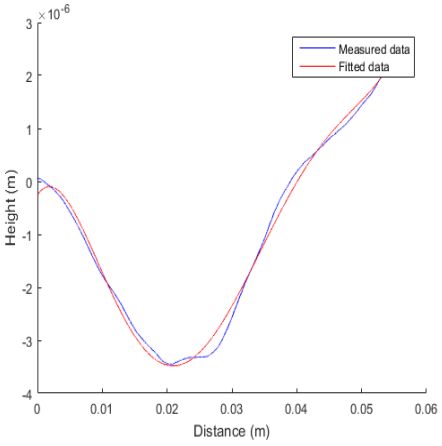

(f) Curvature as a function of distance, Sample S0907

Figure 13.1: Curvature as a function of distance before deposition, 1 of 2

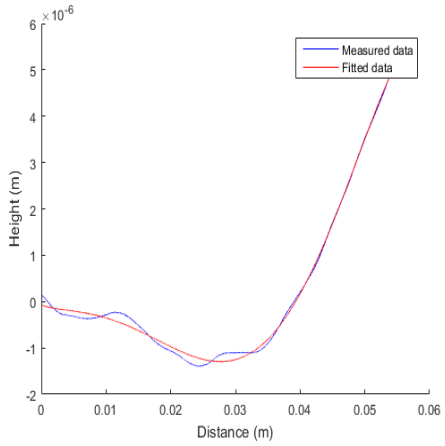

(a) Curvature as a function of distance, Sample S0909

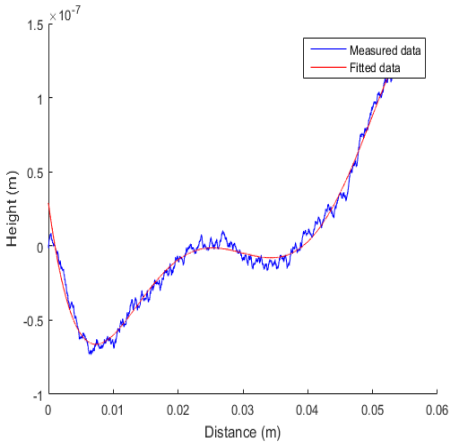

(b) Curvature as a function of distance, Sample S0910

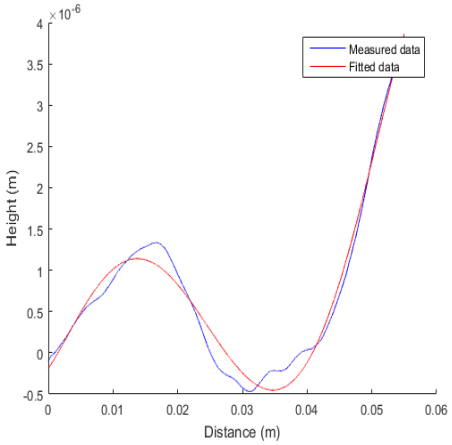

(c) Curvature as a function of distance, Sample S0911

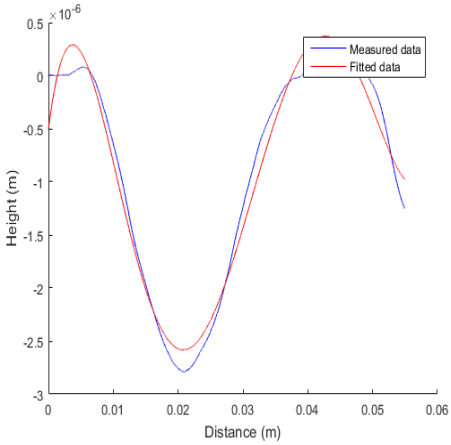

(d) Curvature as a function of distance, Sample S0912

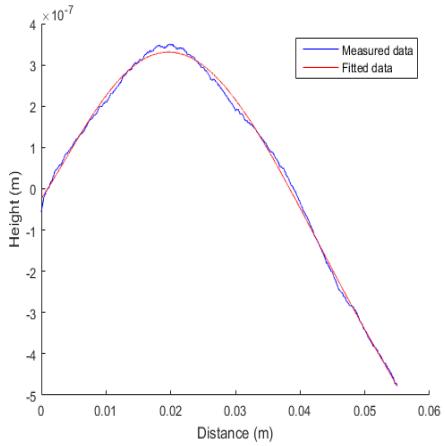

(e) Curvature as a function of distance, Sample S0913

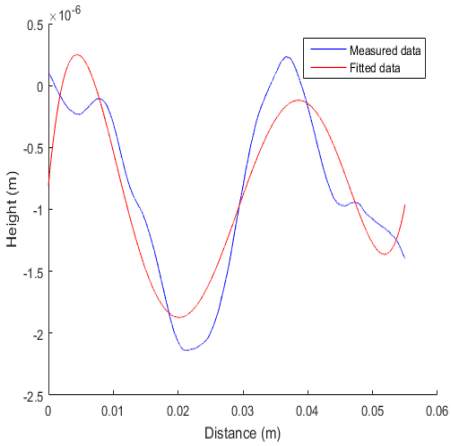

(f) Curvature as a function of distance, Sample S0914

Figure 13.2: Curvature as a function of distance before deposition, 2 of 2

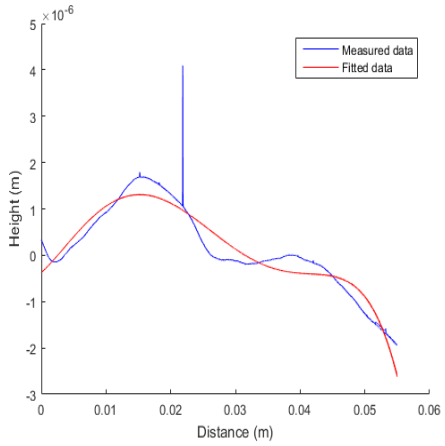

(a) Curvature as a function of distance, Sample S0902

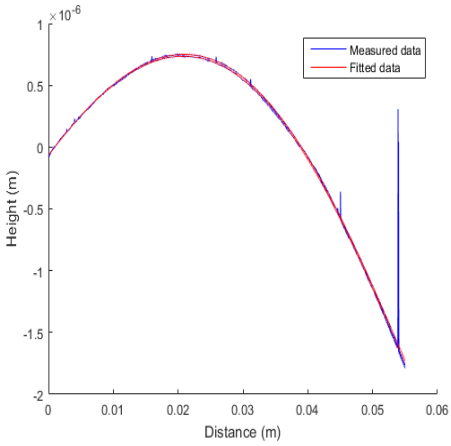

(b) Curvature as a function of distance, Sample S0903

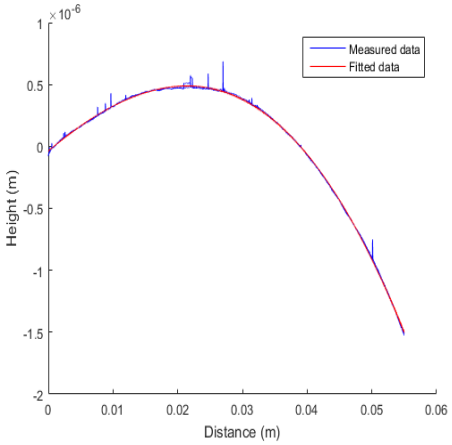

(c) Curvature as a function of distance, Sample S0904

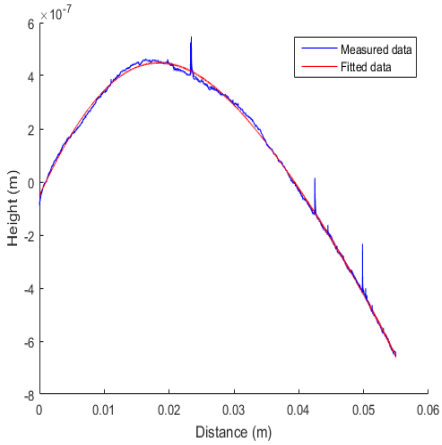

(d) Curvature as a function of distance, Sample S0905

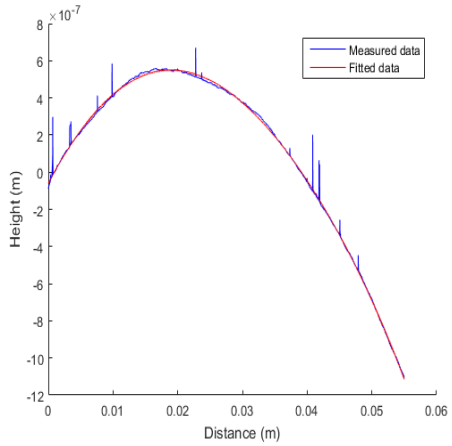

(e) Curvature as a function of distance, Sample S0906

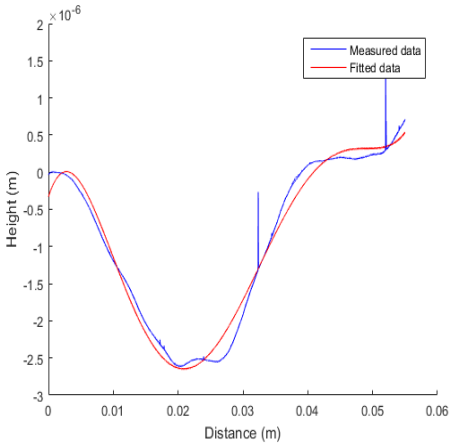

(f) Curvature as a function of distance, Sample S0907

Figure 13.3: Curvature as a function of distance after deposition, 1 of 2

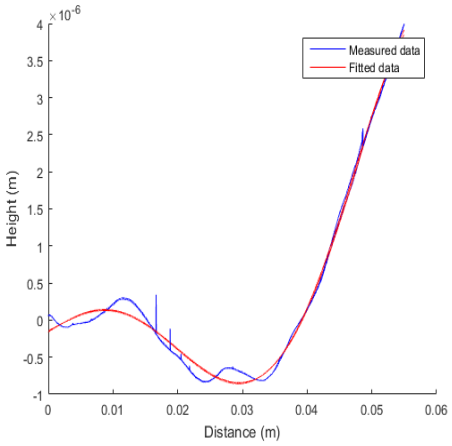

(a) Curvature as a function of distance, Sample S0909

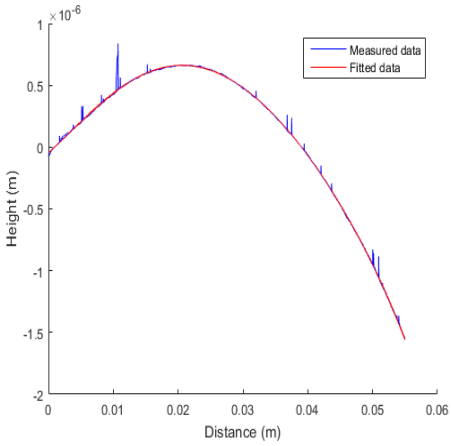

(b) Curvature as a function of distance, Sample S0910

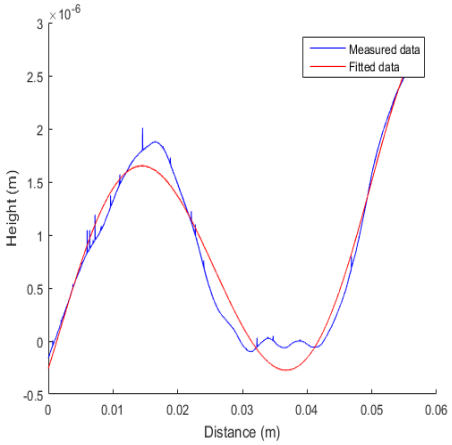

(c) Curvature as a function of distance, Sample S0911

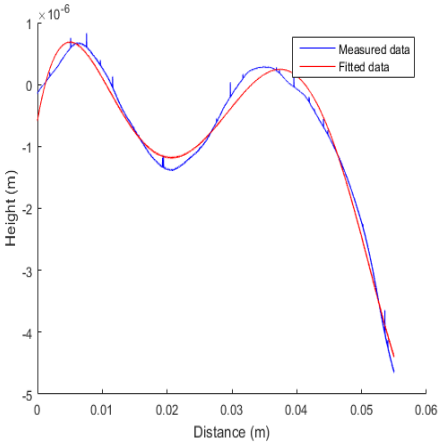

(d) Curvature as a function of distance, Sample S0912

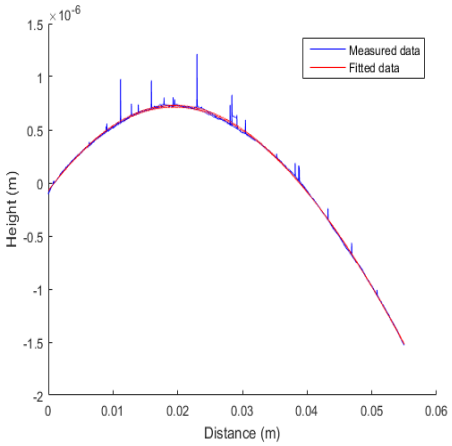

(e) Curvature as a function of distance, Sample S0913

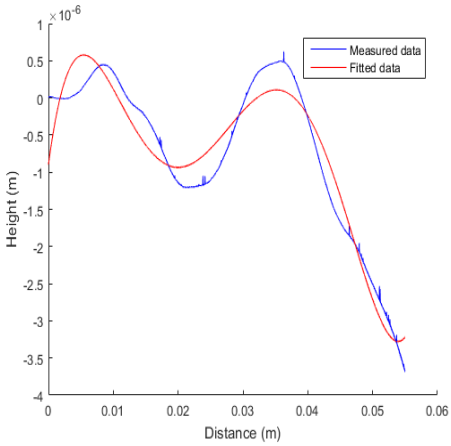

(f) Curvature as a function of distance, Sample S0914

Figure 13.4: Curvature as a function of distance after deposition, 2 of 2

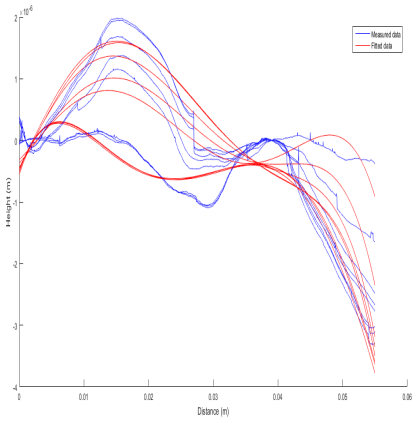

(a) Curvature as a function of distance, Temperature 50°Celsius, Sample S0902

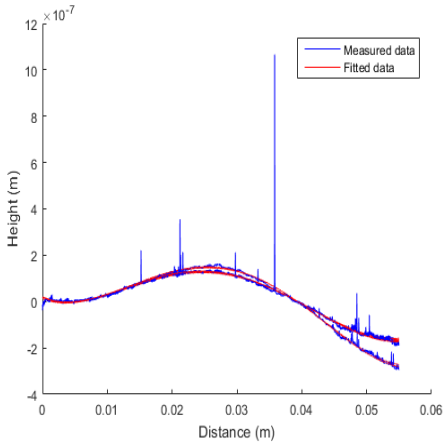

(b) Curvature as a function of distance, Temperature 200°Celsius, Sample S0903

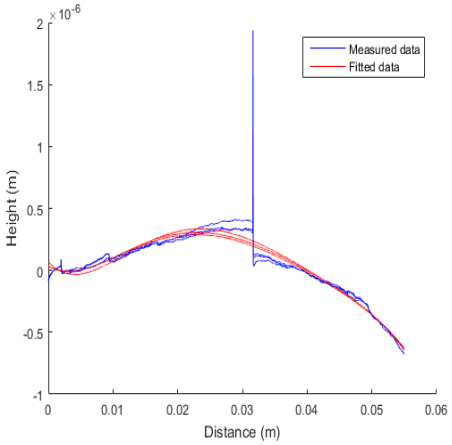

(c) Curvature as a function of distance, Temperature 100°Celsius, Sample S0904

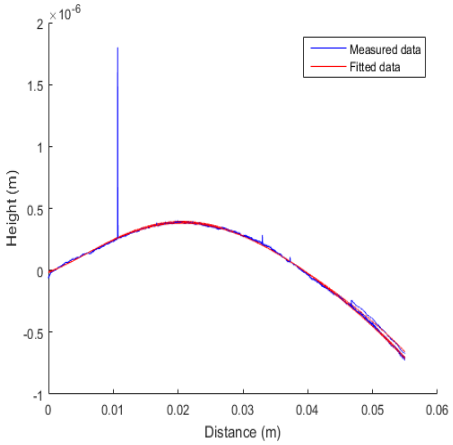

(d) Curvature as a function of distance, Temperature 150°Celsius, Sample S0905

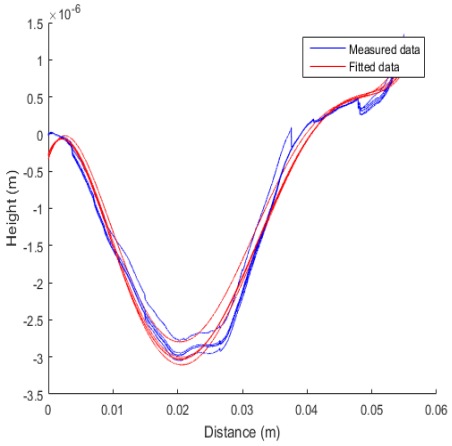

(e) Curvature as a function of distance, Temperature 50°Celsius, Sample S0907

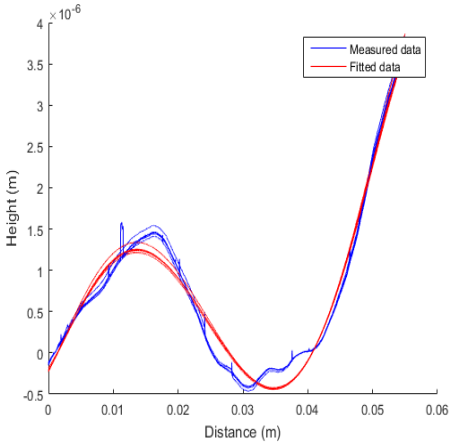

(f) Curvature as a function of distance, Temperature 75°Celsius, Sample S0911

Figure 13.5: Curvature as a function of distance after heating

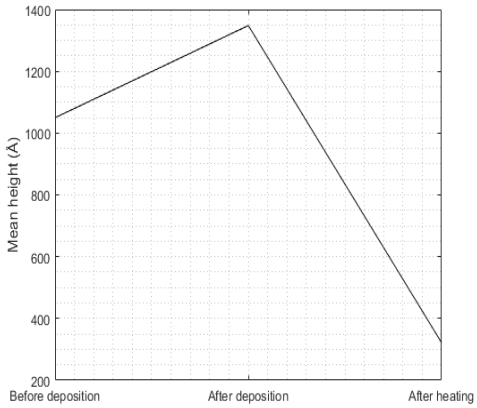

(a) Mean height, Temperature 50°Celsius, Sample S0902

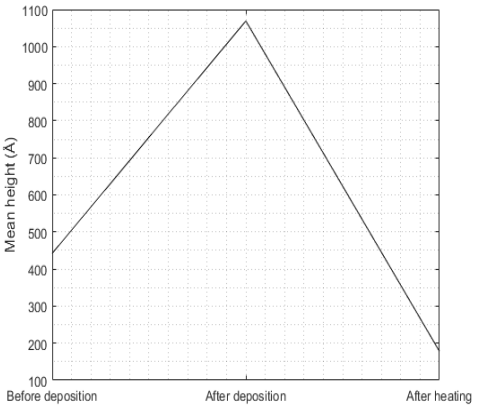

(b) Mean height, Temperature 200°Celsius, Sample S0903

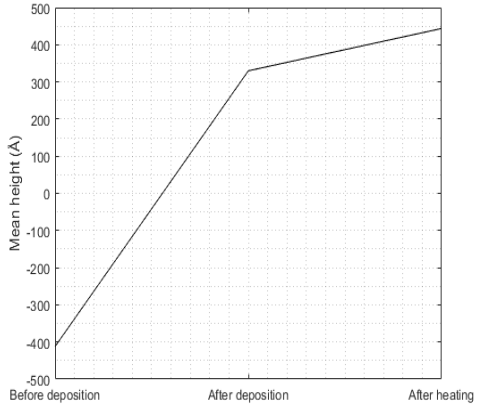

(c) Mean height, Temperature 100°Celsius, Sample S0904

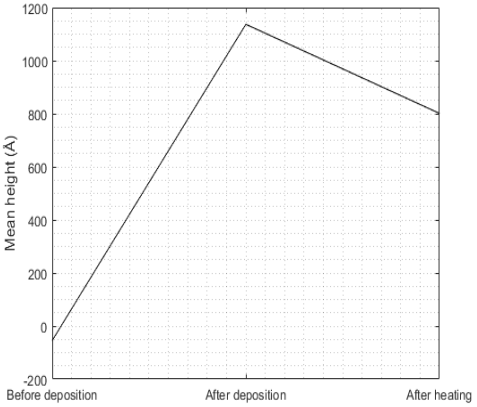

(d) Mean height, Temperature 150°Celsius, Sample S0905

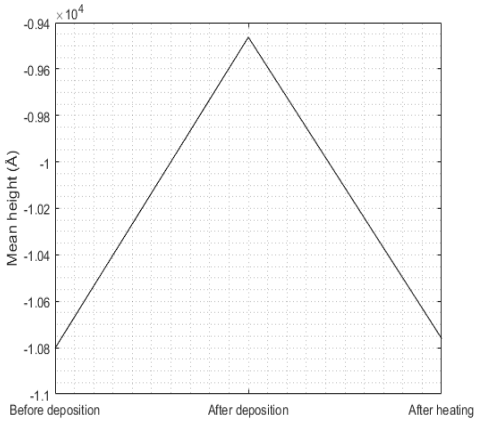

(e) Mean height, Temperature 50°Celsius, Sample S0907

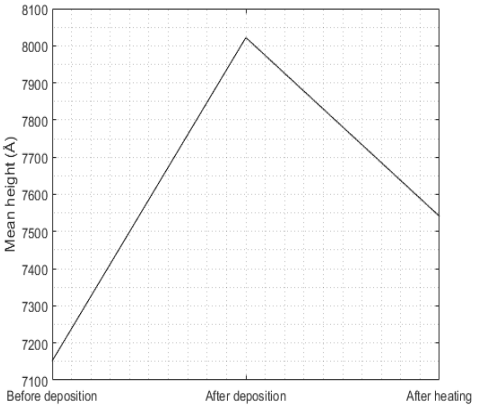

(f) Mean height, Temperature 75°Celsius, Sample S0911

Figure 13.6: Mean height of the curvature, before deposition, after deposition and after heating

14 | Appendix D

01-06-17 15:04 C:\Users\Nis\Desktop\st...\StressTestBC.m 1 of 3

```
close all

%Loading sample by name
SampleName = 's0902';
filename1 = strcat(SampleName, '_b1', '.csv');
filename2 = strcat(SampleName, '_b2', '.csv');
filename3 = strcat(SampleName, '_c1', '.csv');
filename4 = strcat(SampleName, '_c2', '.csv');


filename = {filename1, filename2, filename3, filename4}; %Putting files into an Array


sigma = zeros(4,1);         %Making an empty vector for later, when saving sigma↙
values

for i=1:2
data = csvread(filename{i},19);            %%Reads the datafile from row 19

figure(1)
hold on

x=data(:,1)./(10^6);            %Splitting the data up in two vectors x & y
y=data(:,2)./(10^9);
%Plots the meassured data
plot(x,y,'color','blue');
ylabel('Height (m)');
xlabel('Distance (m)');


p = polyfit(x,y,5);                %%Polyfit fits a polynomium of 5'th grade


q = polyder(p);                     %%Differentiate the poly - Finds y'


h = polyder(q);                 %Differentiates once more - Find y''

Rpre = [];          %Creates empty arrays
y1 = [];

%For Loop that runs through X data and calculates Rpre
    for j = 1:length(y)

        pol1 = q(1)*x(j)^4+q(2)*x(j)^3+q(3)*x(j)^2+q(4)*x(j)+q(5);

        pol2 = h(1)*x(j)^3+h(2)*x(j)^2+h(3)*x(j)+h(4);

        Rpre(j) = ((1+pol1^2)^(3/2))/pol2;

        y1(j) = p(1)*x(j)^5+p(2)*x(j)^4+p(3)*x(j)^3+p(4)*x(j)^2+p(5)*x(j)+p(6);

    end
plot(x,y1,'color','red')          %Plots the simulated data on top of the meassured
%title('Before Coating');
```

Figure 14.1: Matlab script for calculation of stress, page 1 of 3

```
ylabel('Height (m)');
xlabel('Distance (m)');
legend('Measured data','Fitted data','Location','NorthEast')
hold off
R(:,i) = Rpre;
end
sprintf('mean her')
mean(y1)
sprintf('mean her')



for j=3:4
data2 = csvread(filename{j},19);
figure(2)
hold on

x=data2(:,1)./(10^6);
y=data2(:,2)./(10^9);

plot(x,y,'color','blue');
ylabel('Height (m)');
xlabel('Distance (m)');

p = polyfit(x,y,5);

q = polyder(p);

h = polyder(q);

Rpost = [];
y2 = [];

    for k = 1:length(y)

        pol1 = q(1)*x(k)^4+q(2)*x(k)^3+q(3)*x(k)^2+q(4)*x(k)+q(5);

        pol2 = h(1)*x(k)^3+h(2)*x(k)^2+h(3)*x(k)+h(4);

        Rpost(k) = ((1+pol1^2)^(3/2))/pol2;

        y2(k) = p(1)*x(k)^5+p(2)*x(k)^4+p(3)*x(k)^3+p(4)*x(k)^2+p(5)*x(k)+p(6);

    end
plot(x,y2,'color','red')
%title('After Coating');
ylabel('Height (m)');
xlabel('Distance (m)');
legend('Measured data','Fitted data','Location','NorthEast')
hold off
R(:,j) = Rpost;
end


%--------Calculating Stress--------
```

Figure 14.2: Matlab script for calculation of stress, page 2 of 3

```
ts = 500*10^(-6);       %Substrate thickness
tf = 180*10^(-10);      %Film thickness
%E/(1-v)=1.805e11;    %The elasticity
elasticity = 1.805e11;

%Calculating the stress:
sigma_1 = (1/6)*((1./R(:,3)) - (1./R(:,1))) * (elasticity) * (ts^2/tf);
sigma_2 = (1/6)*((1./R(:,4)) - (1./R(:,1))) * (elasticity) * (ts^2/tf);
sigma_3 = (1/6)*((1./R(:,3)) - (1./R(:,2))) * (elasticity) * (ts^2/tf);
sigma_4 = (1/6)*((1./R(:,4)) - (1./R(:,2))) * (elasticity) * (ts^2/tf);

%Taking the mean values of each meassurement
Stress_1 = mean(sigma_1(:,1))*10^(-6)
Stress_2 = mean(sigma_2(:,1))*10^(-6)
Stress_3 = mean(sigma_3(:,1))*10^(-6)
Stress_4 = mean(sigma_4(:,1))*10^(-6)

%Finding the average Stress
sigmastress = (Stress_1+Stress_2+Stress_3+Stress_4)/4
```

Figure 14.3: Matlab script for calculation of stress, page 3 of 3

15 | Appendix E

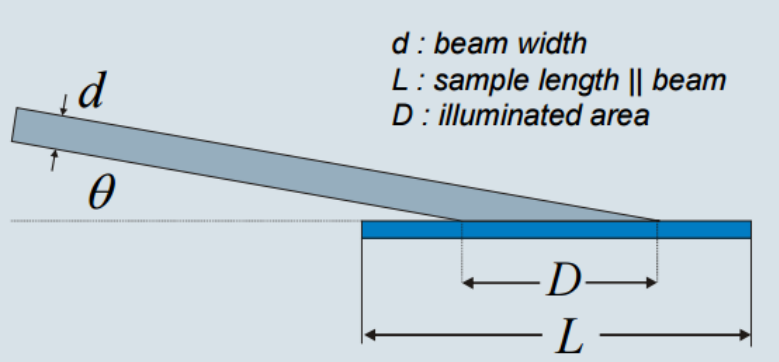

Figure 15.1: Footprint [3]

16 | Appendix F

```
# Nis og Jakob
def onebilayer_Ir_B4C_nj'
        if ($# != 2) {
            eprint "Usage: centerchannel filename"
            exit
      }
      cchan=$1
         newfile $2
         xreju=cchan+100
         xrejl=cchan-100
         xrej xrejl xreju

         mv th 20
         mv tth 40

         #S1
         mv fil -24
         sca2u th -0 -380 tth -0 -760 19 5

         #S2
         mv fil -24
         sca2u th -400 -640 tth -800 -1280 12 5

         #S3
         mv fil -28
         sca2u th -660 -760 tth -1320 -1520 5 5

         #S4
         mv fil -36
         sca2u th -780 -820 tth -1560 -1640 2 5

         #S5
         mv fil -32
         sca2u th -840 -980 tth -1680 -1960 7 5

         #S6
         mv fil -36
         sca2u th -1000 -1060 tth -2000 -2120 3 5

         #S7
         mv fil -40
         sca2u th -1080 -4000 tth -2160 -8000 146 5
         _finish24
'
```

Figure 16.1: XRR-measurement script

17 | Appendix G

Sample	z_{Ir} Å	σ_{Ir} Å	Temperature (°C)	z_{Ir} Å	σ_{Ir} Å
Si6357	93	1.7	50	91	0.9
Si6358	94	2.5	50	93	1.8
Si6359	94	3.1	75	94	0
Si6360	90	0.6	–	–	–
Si6361	92	0	100	93	0
Si6362	95	1.6	100	93	0.4
Si6363	93	0	–	–	–
Si6364	95	1.9	–	–	–
Si6365	94	1.8	150	95	3.1
Si6366	94	2.3	50	93	1.4
Si6367	94	1.4	150	96	3.0
Si6368	94	1.2	–	–	–
Si6369	97	3.7	–	–	–
Si6370	97	2.1	–	–	–
Si6371	95	0	–	–	–
Si6372	98	3.4	200	95	1.0
Si6373	96	2.2	$50-200$	–	–
Si6374	97	1.9	$50-200$	–	–
Si6375	97	1.7	200	96	2.3
Si6376	97	1.6	200	96	1.2
Si6377	–	–	–	–	–
Si6378	97	2.5	200	97	3.5
Si6379	–	–	–	–	–
Si6380	95	2.7	–	–	–
Si6381	92	0	–	9	1.
Si6382	92	1.0	–	9	1.

Table 17.1: Calculated Ir thickness and Ir/B_4C interface roughness before and after heating

18 | Appendix H

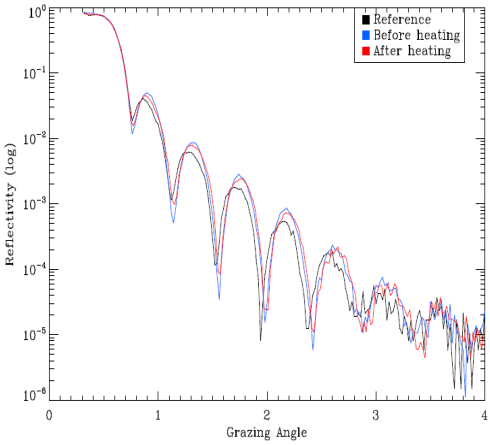

(a) XRR measurement, before and after heating, Temperature 50°C, Sample Si6357

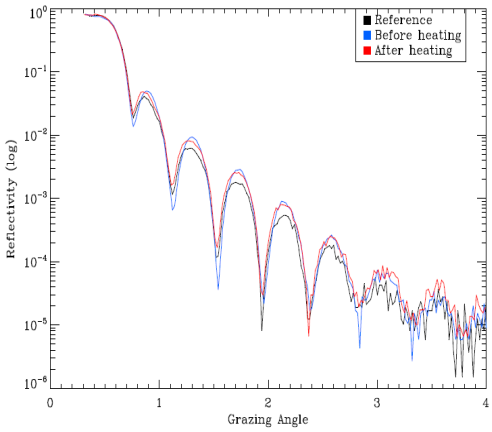

(b) XRR measurement, before and after heating, Temperature 75°C, Sample Si6359

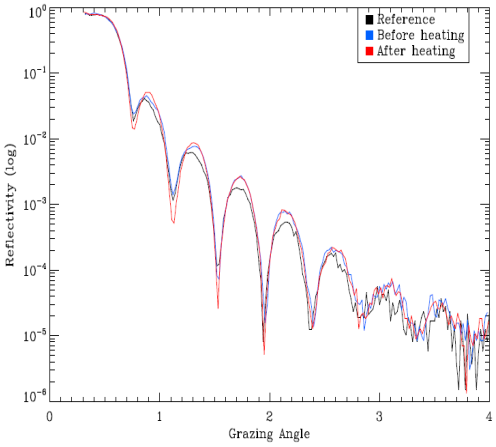

(c) XRR measurement, before and after heating, Temperature 100°C, Sample Si6361

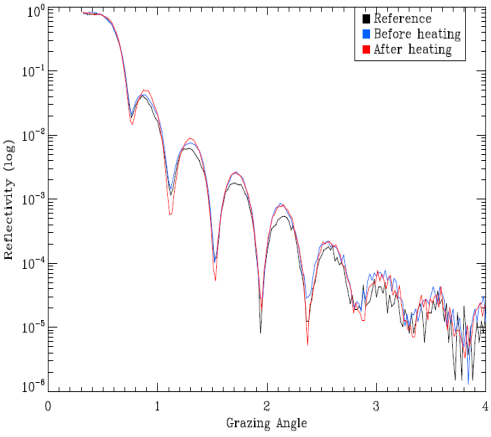

(d) XRR measurement, before and after heating, Temperature 100°C, Sample Si6362

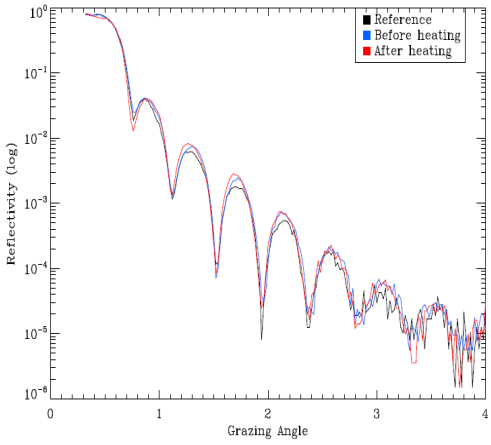

(e) XRR measurement, before and after heating, Temperature 150°C, Sample Si6365

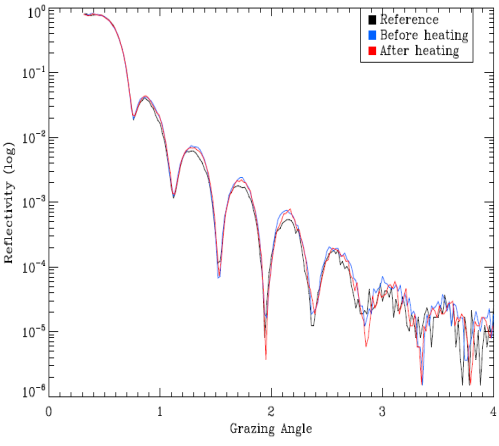

(f) XRR measurement, before and after heating, Temperature 50°C, Sample Si6366

Figure 18.1: XRR measurement, before and after heating, 1 of 2

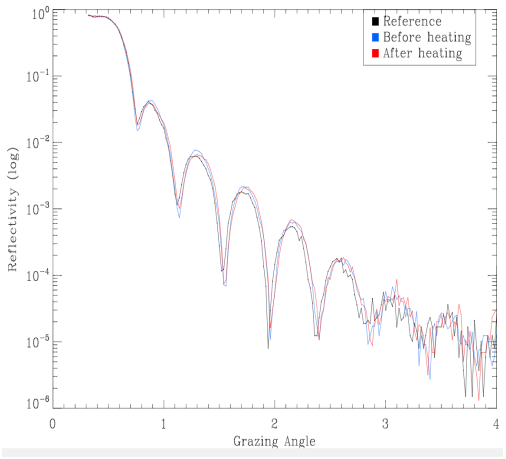

(a) XRR measurement, before and after heating, Temperature 50°C, Sample Si6358

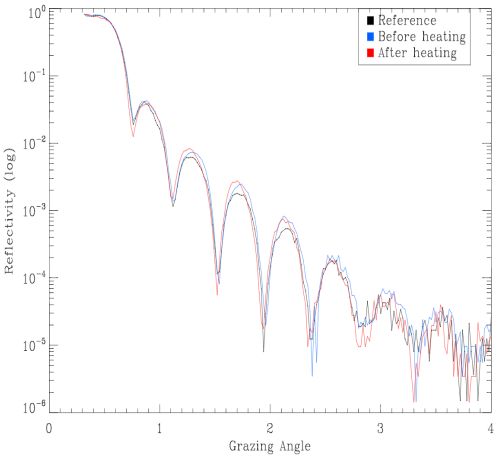

(b) XRR measurement, before and after heating, Temperature 150°C, Sample Si6367

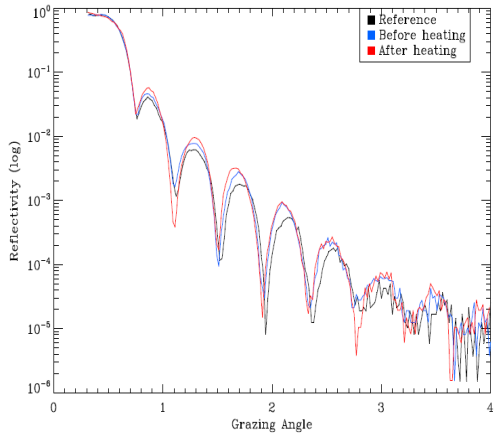

(c) XRR measurement, before and after heating, Temperature 200°C, Sample Si6372

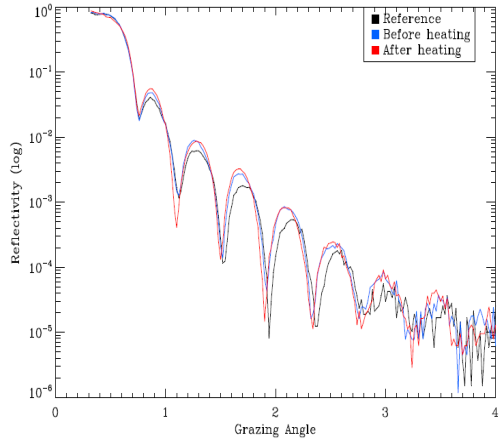

(d) XRR measurement, before and after heating, Temperature 200°C, Sample Si6375

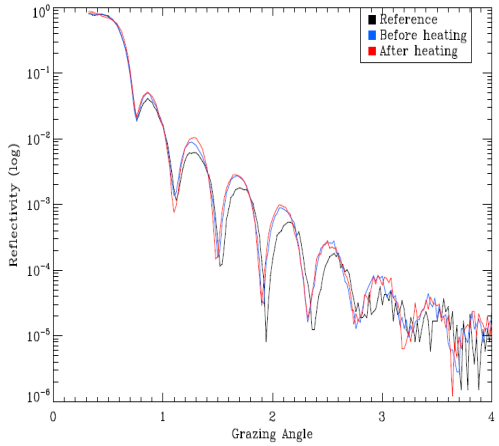

(e) XRR measurement, before and after heating, Temperature 200°C, Sample Si6376

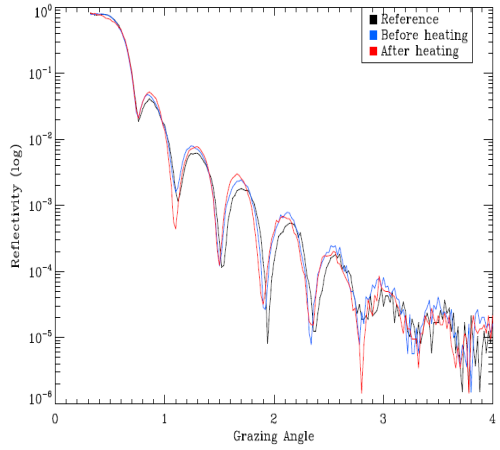

(f) XRR measurement, before and after heating, Temperature 200°C, Sample Si6378

Figure 18.2: XRR measurement, before and after heating, 2 of 2

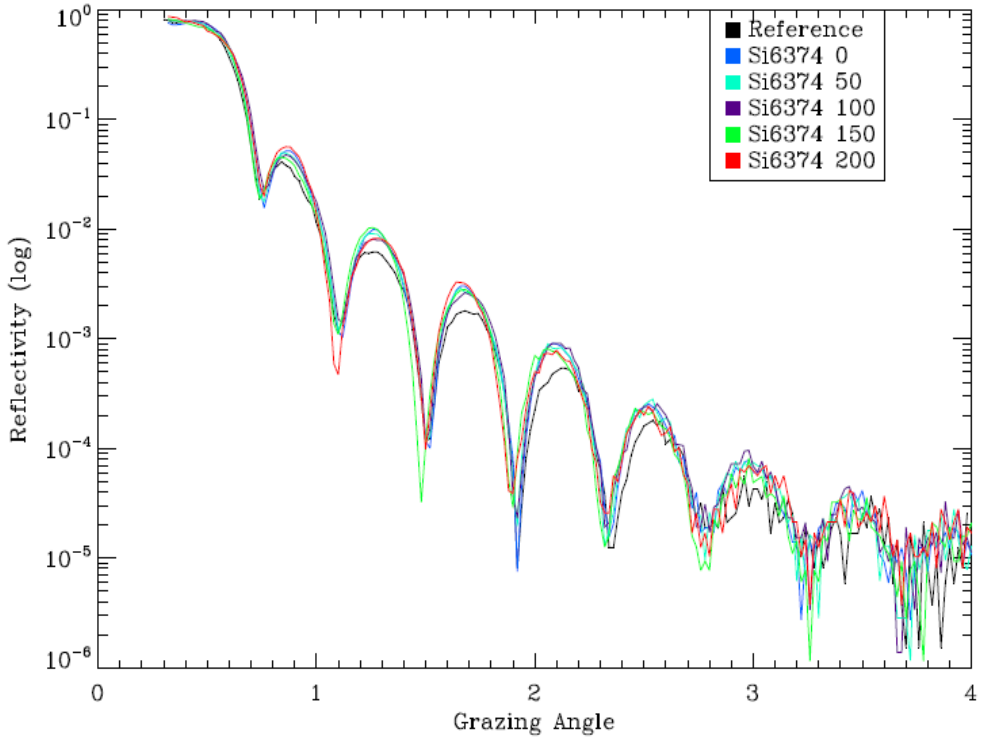

(a) XRR measurement, before and after heating, Temperature 50-200°C, Sample Si6373

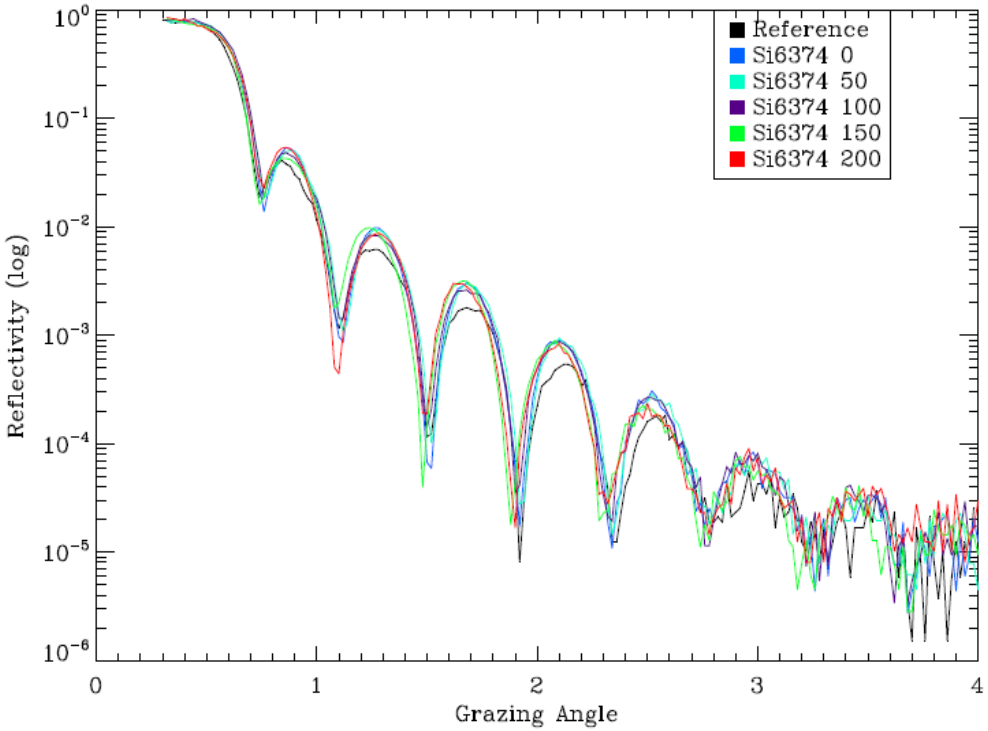

(b) XRR measurement, before and after heating, Temperature 50-200°C, Sample Si6374

Figure 18.3: Cumulative XRR measurement, before and after heating

19 | Appendix I

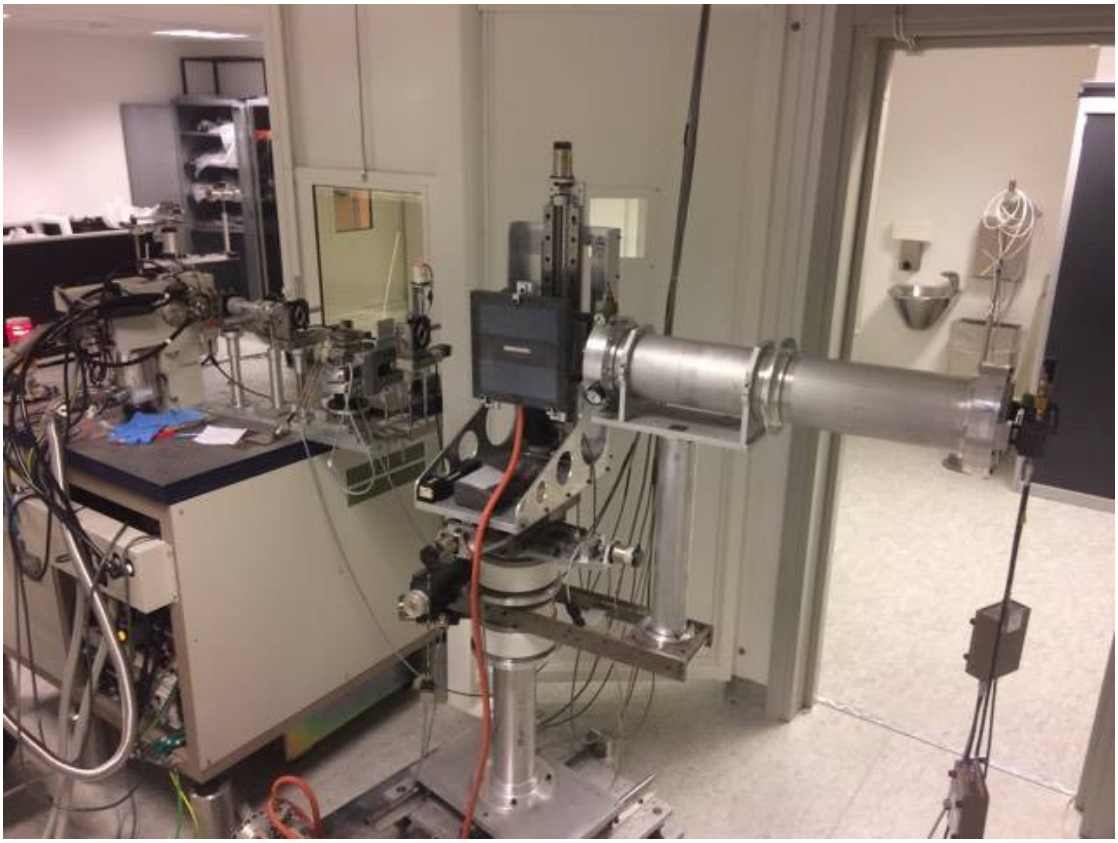

Figure 19.1: XRR facility

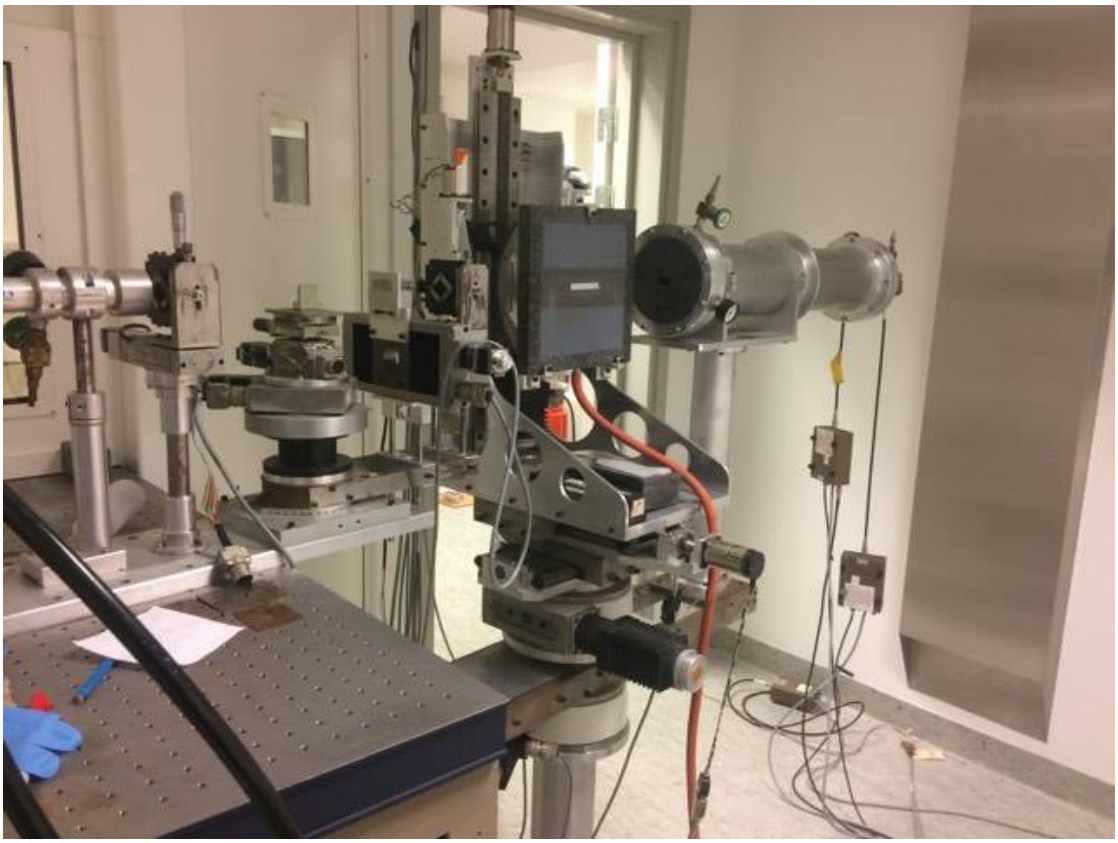

Figure 19.2: XRR facility

20 | Appendix J

```
.r rdtab
.r BIocarray
.r Ir_B4C_SiO

; Loading data
print, '----------Before heating----------'
data=rdtab('./data/si6374_1.txt')       ;Insert you
r file name at "test.txt"

xxB = data(0,*)             ;Loads first colum "the
ta" into xxB
yyB = data(1,*)             ;Loads second colum "re
flectivity" into yyB
erB = data(2,*)             ;Loads third colum "err
ors" into erB

i= where(yyB gt 0. and xxB gt 0.3 and xxB le 4.)
  ;Tells that yyB has to be greater than 0, and xx
B                           ;greater than 0, less
than 5.

xx=xxB(i)               ;Loads the data into xx,yy,
erY with i as bla bla
yy=yyB(i)
erY=erB(i)
;-----
; Creating a model

energy=8.047                ;keV
hc = 4.1356692e-15              ;Planck's constant
, in eV
lightS = 299792458.               ;Speed of light,
 in m/s
Lambda = ((hc*lightS)*1e7)/(energy)   ;in Ã¥ngstron
s
sigma = [2.5, 2.5, 2.5]         ;Sigma is locked fo
r now
theta = xx              ;naming the values correctl
y
nLayer = 2              ;How many layers you have
optCte = Ir_B4C_SiO(Lambda)         ;Calling the Ir
```

Figure 20.1: IDL script, page 1 of 7

```
_B4C_SiO function with lambda
NC = BIocarray(optCte, Lambda)      ;Calculates the
 optical constants

list2 = LIST()
s = 0.+findgen(81)*0.1
a = 1.+findgen(25)*0.25
list = LIST()
x = 0.+findgen(41)*5
y = 0.+findgen(201)*1

;-------------- Calculating the best fit
;for i=0, N_ELEMENTS(x)-1 do begin &$
    for j = 0, N_ELEMENTS(y)-1 do begin  &$
              z = [80., y(j)] &$
              for l = 0, N_ELEMENTS(s)-1 do begin &$
                  ;for o = 0, N_ELEMENTS(a)-1 do begi
n &$
                           sigma = [2.5, s(l), 2.5] &$

                           FRESNEL, (90-theta), LAMBDA
, NC, Z, SIGMA, RA=RA &$
                           result = TOTAL((ra-yy)^2/yy
) &$
                           list.Add, [sigma(1), sigma(
2), z, result] &$
                  ;endfor &$
              endfor &$
    endfor &$
;endfor &$
print, 'Done with loop'

k = list.ToArray()

minindex = MIN(k[*,4],I, DIMENSION=1)

final = k[I,*]

z = [final(2), final(3)]

sigma = [2.5, final(0), final(1)]
```

Figure 20.2: IDL script, page 2 of 7

```
FRESNEL, (90-theta), LAMBDA, NC, Z, SIGMA, RA=RA  ;
Calls out the Fresnel function.

print, 'Thickness =', z

print, 'Roughness =', sigma

print, 'Chi Square=', final(4)

result2 = TOTAL((ra-yy)^2/yy)

print, 'Best Chi Square=', result2

;---------------------------------After heating sam
ple
print, '----------After heating----------'
data=rdtab('./data/si6374a_2.txt')      ;Insert you
r file name at "test.txt"

xxB = data(0,*)             ;Loads first colum "the
ta" into xxB
yyB = data(1,*)             ;Loads second colum "re
flectivity" into yyB
erB = data(2,*)             ;Loads third colum "err
ors" into erB

i= where(yyB gt 0. and xxB gt 0.3 and xxB le 4.)
  ;Tells that yyB has to be greater than 0, and xx
B                           ;greater than 0, less
than 5.

xx=xxB(i)               ;Loads the data into xx,yy,
erY with i as bla bla
yy=yyB(i)
erY=erB(i)
;-----
; Creating a model

energy=8.047                ;keV
hc = 4.1356692e-15              ;Planck's constant
, in eV
lightS = 299792458.               ;Speed of light,
```

Figure 20.3: IDL script, page 3 of 7

```
 in m/s
Lambda = ((hc*lightS)*1e7)/(energy)   ;in Ã¥ngstron
s
sigma = [2.5, 2.5, 2.5]         ;Sigma is locked fo
r now
theta = xx              ;naming the values correctl
y
nLayer = 2              ;How many layers you have
optCte = Ir_B4C_SiO(Lambda)         ;Calling the Ir
_B4C_SiO function with lambda
NC = BIocarray(optCte, Lambda)      ;Calculates the
 optical constants

list2 = LIST()
s = 0.+findgen(81)*0.1
a = 1.+findgen(25)*0.25
list = LIST()
x = 0.+findgen(41)*5
y = 0.+findgen(201)*1

;--------------- Calculating the best fit
;for i=0, N_ELEMENTS(x)-1 do begin &$
    for j = 0, N_ELEMENTS(y)-1 do begin  &$
             z = [80., y(j)] &$
             for l = 0, N_ELEMENTS(s)-1 do begin &$
                 ;for o = 0, N_ELEMENTS(a)-1 do begi
n &$
                         sigma = [2.5, s(l), 2.5] &$

                         FRESNEL, (90-theta), LAMBDA
, NC, Z, SIGMA, RA=RA &$
                         result = TOTAL((ra-yy)^2/yy
) &$
                         list.Add, [sigma(1), sigma(
2), z, result] &$
                 ;endfor &$
             endfor &$
    endfor &$
;endfor &$
print, 'Done with loop'

k = list.ToArray()
```

Figure 20.4: IDL script, page 4 of 7

```
minindex = MIN(k[*,4],I, DIMENSION=1)

final = k[I,*]

z = [final(2), final(3)]

sigma = [2.5, final(0), final(1)]

FRESNEL, (90-theta), LAMBDA, NC, Z, SIGMA, RA=RA  ;
Calls out the Fresnel function.

print, 'Thickness =', z

print, 'Roughness =', sigma

print, 'Chi Square=', final(4)

result2 = TOTAL((ra-yy)^2/yy)

print, 'Best Chi Square=', result2

;----------------------------Plotting reference sa
mple together with before and after heating for a
sample
; Loading data
data=rdtab('./data/si6380_1.txt')       ;Insert you
r file name at "test.txt"

xxB = data(0,*)             ;Loads first colum "the
ta" into xxB
yyB = data(1,*)             ;Loads second colum "re
flectivity" into yyB
erB = data(2,*)             ;Loads third colum "err
ors" into erB

i= where(yyB gt 0. and xxB gt 0.3 and xxB le 5.)
  ;Tells that yyB has to be greater than 0, and xx
B                           ;greater than 0, less
than 5.

xx=xxB(i)               ;Loads the data into xx,yy,
```

Figure 20.5: IDL script, page 5 of 7

```
erY with i as bla bla
yy=yyB(i)
erY=erB(i)
;erY(0:99)=1/erY(0:99)              ;0 - 2
;erY(0:124)=1/erY(0:124)        ; 0 - 2.5
;-----

set_plot,'ps'
device,filename= './si6380_74_74a_200',/color
loadct, 13

plot, xx, yy, /ylog, psym=3, ytitle='!6Reflectivity
 (log)', xtitle='!6Grazing Angle'
oplot, xx, yy
;errplot, xx,yy-erY, yy+erY ;errplot - Plots the er
rorbars onto the plot

;--------------

data=rdtab('./data/si6374_1.txt')       ;Insert you
r file name at "test.txt"

xxB = data(0,*)             ;Loads first colum "the
ta" into xxB
yyB = data(1,*)             ;Loads second colum "re
flectivity" into yyB
erB = data(2,*)             ;Loads third colum "err
ors" into erB

i= where(yyB gt 0. and xxB gt 0.3 and xxB le 5.)
  ;Tells that yyB has to be greater than 0, and xx
B                           ;greater than 0, less
than 5.

xx=xxB(i)               ;Loads the data into xx,yy,
erY with i as bla bla
yy=yyB(i)
erY=erB(i)
;erY(0:99)=1/erY(0:99)              ;0 - 2
;erY(0:124)=1/erY(0:124)        ; 0 - 2.5
;-----
```

Figure 20.6: IDL script, page 6 of 7

```
oplot, xx, yy, color=80
;errplot, xx,yy-erY, yy+erY, color=80 ;errplot - Pl
ots the errorbars onto the plot


;--- Loading data

data=rdtab('./data/si6374a_13.txt')     ;Insert you
r file name at "test.txt"

xxB = data(0,*)             ;Loads first colum "the
ta" into xxB
yyB = data(1,*)             ;Loads second colum "re
flectivity" into yyB
erB = data(2,*)             ;Loads third colum "err
ors" into erB

i= where(yyB gt 0. and xxB gt 0.3 and xxB le 5.)
  ;Tells that yyB has to be greater than 0, and xx
B                           ;greater than 0, less
than 5.

xx=xxB(i)               ;Loads the data into xx,yy,
erY with i as bla bla
yy=yyB(i)
erY=erB(i)
oplot, xx, yy, color=300
;errplot, xx,yy-erY, yy+erY, color=300 ;errplot - P
lots the errorbars onto the plot
legend,["!6Reference","Before heating","After heat
ing"],PSym=[8,8,8],color=[0,80,300], position=[2.8
,1]


device, /close
set_plot, 'x'
loadct, 10
```

Figure 20.7: IDL script, page 7 of 7